Persistent Global Greening Over the Last Four Decades Using Novel Long-term Vegetation Index Data with Enhanced Temporal Consistency

Sungchan Jeong[a,b], Youngryel Ryu[a,b,c*], Pierre Gentine[e,f], Xu Lian[e], Jianing Fang[e], Xing Li[d], Juwon Kong[d], Wonseok Choi[a,b], Chongya Jiang[g,h], Trevor Keenan[i,j], Sandy P. Harrison[k], Iain Colin Prentice[l]

a. Interdisciplinary Program in Landscape Architecture, Seoul National University, Seoul, Republic of Korea

b. Integrated Major in Smart City Global Convergence, Seoul National University, Seoul, Republic of Korea

c. Department of Landscape Architecture and Rural Systems Engineering, Seoul National University, Seoul, Republic of Korea

d. Research Institute of Agriculture and Life Sciences, Seoul National University, Seoul, Republic of Korea

e. Department of Earth and Environmental Engineering, Columbia University, New York, NY, USA

f. Center for Learning the Earth with Artificial intelligence and Physics (LEAP), Columbia University, New York, NY, USA.

g. Agroecosystem Sustainability Center, Institute for Sustainability, Energy, and Environment, University of Illinois at Urbana Champaign, Urbana, IL, USA.

h. Department of Natural Resources and Environmental Sciences, College of Agricultural, Consumer and Environmental Sciences, University of Illinois at Urbana Champaign, Urbana, IL, USA

i. Climate and Ecosystem Sciences Division, Lawrence Berkeley National Laboratory, Berkeley, CA, USA

j. Department of Environmental Science, Policy and Management, UC Berkeley, Berkeley, CA, USA

k. Geography and Environmental Science, University of Reading, Whiteknights, Reading RG6 6AH, United Kingdom

l. Georgina Mace Centre for the Living Planet, Department of Life Sciences, Imperial College London, Silwood Park Campus, Buckhurst Road, Ascot SL5 7PY, United Kingdom

*corresponding author: Youngryel Ryu (ryuyr77@gmail.com)

This is a non-peer reviewed preprint submitted to EarthArXiv.

Abstract

Advanced Very High-Resolution Radiometer (AVHRR) satellite observations have provided the longest global daily records from 1980s, but the remaining temporal inconsistency in vegetation index datasets has hindered reliable assessment of vegetation greenness trends. To tackle this, we generated novel global long-term Normalized Difference Vegetation Index (NDVI) and Near-Infrared Reflectance of vegetation (NIRv) datasets derived from AVHRR and Moderate Resolution Imaging Spectroradiometer (MODIS). We addressed residual temporal inconsistency through three-step post processing including cross-sensor calibration among AVHRR sensors, orbital drifting correction for AVHRR sensors, and machine learning-based harmonization between AVHRR and MODIS. After applying each processing step, we confirmed the enhanced temporal consistency in terms of detrended anomaly, trend and interannual variability of NDVI and NIRv at desert calibration sites. Our refined NDVI and NIRv datasets showed a persistent global greening trend over the last four decades (NDVI: 0.0008 yr^{-1}; NIRv: 0.0003 yr^{-1}), contrasting with those without the three processing steps that showed rapid greening trends before 2000 (NDVI: 0.0017 yr^{-1}; NIRv: 0.0008 yr^{-1}) and weakened greening trends after 2000 (NDVI: 0.0004 yr^{-1}; NIRv: 0.0001 yr^{-1}). These findings highlight the importance of minimizing temporal inconsistency in long-term vegetation index datasets, which can support more reliable trend analysis in global vegetation response to climate changes.

Key words: AVHRR, MODIS, NDVI, NIRv, greening trend, orbital drift

1 Introduction

There has been growing debates on the trend of global vegetation greenness and its relation with climate change (Piao et al., 2020). For example, a recent study reported a sharp declining trend in the global CO_2 fertilization effect on vegetation photosynthesis (Wang et al., 2020). However, subsequent commentary papers raised concerns about technical issues in Advanced Very High-Resolution Radiometer (AVHRR) Near-Infrared Reflectance of vegetation (NIRv) datasets (Frankenberg et al., 2021; Zhu et al., 2021), which is strong proxy of vegetation photosynthesis (Badgley et al., 2019; Dechant et al., 2020). Frankenberg et al. (2021) reported artefacts in AVHRR NIRv datasets stemmed from inconsistent biases between AVHRR sensors and the orbital drifting effect. Zhu et al. (2021) reported that the harmonized Moderate Resolution Imaging Spectroradiometer (MODIS) NIRv used by Wang et al. (2020) exhibited a smaller greening trend and reduced interannual variations compared to the original MODIS NIRv. Through these studies, we have learned not only the strength of long-term analysis with AVHRR observations but also the importance of rigorous data processing to minimize residual artefacts. Consequently, further steps are imperative in addressing the identified uncertainties including inconsistent bias between different sensors, orbital drifting effect, and inappropriate harmonization with other satellites. By examining the effects of these uncertainties on vegetation index trends, we can gain a more robust understanding of global long-term vegetation dynamics.

Since the early 1980s, AVHRR on board the National Oceanic and Atmospheric Administration (NOAA) polar-orbiting environmental satellites has provided the longest data records of global satellite measurements on land surface (Pedelty et al., 2007; Franch et al., 2017; Vermote, 2021; Santamaria-Artigas et al., 2021). Long-term AVHRR observations have been widely used to derive vegetation products, including NDVI (Tucker et al., 2005; Pinzon and Tucker, 2014), NIRv (Wang et al., 2020), leaf area index (LAI), fraction of photosynthetically active radiation (FPAR) (Myneni et al., 1997; Liu et al., 2012; Zhu et al., 2013; Xiao et al., 2016), and gross primary production (GPP) (Smith et al., 2016; Wang et al., 2021). These AVHRR products have played a crucial role in understanding global terrestrial carbon cycle and climate feedback (Zhu et al., 2016; Keenan et al., 2016; Chen et al., 2019;

Piao et al., 2020).

In particular, relentless efforts have led to considerable improvement in AVHRR vegetation index datasets (Pinzon and Tucker, 2014; Zhu et al., 2013; Xiao et al., 2016). The Global Inventory Modeling and Mapping Studies (GIMMS) NDVI applied Bayesian methods with high-quality NDVI data from the Sea-Viewing Wide Field-of-view Sensor (Pinzon and Tucker, 2014). While GIMMS NDVI had the highest temporal consistency among the four long-term AVHRR-based NDVI datasets, residual orbital drift effects and sensor degradation may lead to temporal inconsistency (Tian et al., 2015). Recently, Li et al. (2023) improved temporal consistency of GIMMS3g NDVI (PKU GIMMS) by calibrating GIMMS3g NDVI with Landsat and MODIS NDVI. AVHRR Long-Term Data Record (LTDR) team has provided a high-quality Bi-directional Reflectance Distribution Function (BRDF) normalized daily surface reflectance, which is a unique source for investigating long-term vegetation index from the spectral reflectance level (Pedelty et al., 2007; Franch et al., 2017; Santamaria-Artigas et al., 2021). In the case of LTDR V3, Nagol et al. (2014) demonstrated that the application of BRDF correction had led to a substantial reduction in spurious inter-annual NDVI trends. Franch et al. (2017) reported improved data quality of LTDR V4 BRDF normalized reflectance with geolocation correction and cloud mask improvement by evaluating it against in-situ data and MODIS surface reflectance. Enhancements in the LTDR V5 encompassed BRDF correction, calibration, and atmospheric correction with improved quality assessment flags (Vermote et al., 2021; https://landweb.modaps.eosdis.nasa.gov/). A recent study comprehensively evaluated LTDR V5 spectral reflectance using Landsat-5 surface reflectance and reported enhanced performance with improved BRDF correction (Santamaria-Artigas et al., 2021).

However, studies have still pointed out remaining issues regarding temporal inconsistency in AVHRR vegetation index datasets (Giglio and Roy, 2020; Zhu et al., 2021; Frankenberg et al., 2021). The first issue contributing to temporal inconsistency was the inconsistent biases between AVHRR sensors identified at pseudo-invariant calibration sites (PICS). Earlier studies found that inconsistent bias between AVHRR sensors introduced notable temporal inconsistency in spectral reflectance (Latifovic et al., 2012; Li et al., 2014). Recent studies still reported residual temporal inconsistency in spectral reflectance and vegetation index across successive AVHRR sensors over desert calibration sites (Giglio and Roy, 2020; Frankenberg et al., 2021). Especially, Frankenberg et al. (2021) reported that variations in detrended global mean AVHRR NIRv were closely similar to those found in PICS.

The second issue was orbital drifting effects on spectral reflectance and vegetation index. The orbital drifting effect means that changes in the local overpass time of sensors lead to changes in the solar zenith angle (SZA). This poses an issue, as the surface reflectance over anisotropic surfaces varies depending on the SZA (Fensholt et al., 2009; Nagol et al., 2014; Roy et al., 2020). Orbital drifting effects on spectral reflectance and vegetation index vary depending on ecosystems due to different surface anisotropic characteristics (Gutman, 1999; Los et al., 2005). For example, evergreen needleleaf forest showed a positive relationship between NDVI and SZA due to the larger reduction of red reflectance than near-infrared (NIR) reflectance with increasing SZA, while deciduous broadleaf forest did not show a clear relationship between NDVI and SZA (Deering et al., 1999). In terms of trend analysis, studies have reported orbital drifting effects across the different AVHRR-based NDVI products and potential uncertainty in NDVI trends across the latitudes (Tian et al., 2015; Beck et al., 2011). For instance, tropical regions near the equator suffered from orbital drifting effects due to a larger annual SZA anomaly than other regions (Tian et al., 2015). Furthermore, a large annual anomaly of SZA in NOAA 07, 09, 11, and 14 had a more notable orbital drifting effect compared to NOAA 16, 18, 19, and MetOP-B which had relatively smaller SZA annual anomaly (Frankenberg et al., 2021).

The last issue was an incomplete harmonization of AVHRR vegetation index with other satellite products. Because of the broad red and NIR wavelength channels in AVHRR sensors, many studies have tried to harmonize AVHRR NDVI with MODIS NDVI, which is designed to better capture vegetation signals with narrow spectral channels (Chen et al., 2019; Zhu et al., 2021). Studies have adopted several approaches to harmonize AVHRR with MODIS including pixel-wise linear model (Mao et al., 2012), and cumulative distribution frequency matching (Wang et al., 2020). But further studies showed that non-linearities between different satellite NDVI products limited a global scale application of the linear model-based approach (Ju et al., 2016; Berner et al., 2020). For this, studies demonstrated the strength of machine learning-based harmonization for addressing the non-linear relationships between different satellite NDVI products (Berner et al., 2020; Li et al., 2023). Recently, Zhu et al. (2021) showed that harmonization of MODIS NIRv with AVHRR NIRv could lead to a large discrepancy in interannual variations and trends due to the uncertainties in AVHRR NIRv dataset. We need to address the ongoing challenges of temporal inconsistency in AVHRR vegetation index datasets for a robust understanding of long-term vegetation trends (Santamaria-Artigas et al., 2021).

In this study, we generated robust NDVI and NIRv datasets based on AVHRR LTDR V5 by addressing temporal inconsistency stemmed from inconsistent biases across AVHRR sensors, the orbital drifting effects, and incomplete harmonization with MODIS. We aimed to enhance the temporal consistency of long-term NDVI and NIRv datasets and to investigate how the resulting vegetation trends change.

2 Materials and Methods

2.1 Data

2.1.1 AVHRR LTDR V5

We used the AVHRR LTDR V5 surface reflectance product (AVH09C1) generated from AVHRR L1b Global Area Coverage (GAC) data for 1982-2021 (Franch et al., 2017; Santamaria-Artigas et al., 2021; Vermote, 2021). LTDR V5 used 8 satellites including NOAA-07, 09, 11, 14, 16, 18, 19, and MetOP-B from June of 1981 to the present day (Table 1). LTDR V5 provides BRDF normalized reflectance which has a daily temporal resolution and 0.05° spatial resolution in the Climate Modeling Grid (CMG). We used BRDF normalized reflectance with fixed geometry (SZA: 45°; VZA: 0°) from red (0.58~0.68 μm) and near-infrared (NIR) (0.72~1.10 μm) channels, SZA at overpass time, and quality assessment layer. The detailed relative spectral responses of each AVHRR satellite were in Fig. A1. We only used valid, cloud-free, and BRDF normalized pixels after filtering the low-quality data using the quality assessment layer. The obvious bad-quality data at the beginning of the NOAA 11 operating period (1988.11–1989.10) reported by Tian et al. (2015) were replaced with an average of the data from the previous and the subsequent year in each month before applying further processing.

Table 1 List of satellites used to process AVHRR LTDR V5 (Vermote et al., 2021)

Satellite	Start (Year, Day of year)	End (Year, Day of year)
NOAA 07	1982, 001	1985, 003
NOAA 09	1985, 004	1988, 312
NOAA 11	1988, 313	1994, 365
NOAA 14	1995, 001	2000, 305
NOAA 16	2000, 306	2005, 365
NOAA 18	2006, 001	2007, 365
NOAA 19	2010, 001	2016, 366
MetOP-B	2017, 001	2021, 365

2.1.2 MODIS

We used MODIS BRDF product (MCD43C1, Collection 6.1) distributed by the Land Processes Distributed Active Archive Center (LP DAAC) (Wang et al., 2018) as a reference for generating consistent long-term vegetation index dataset. MCD43C1 have a daily temporal resolution and 0.05° spatial resolution in the CMG grid. MODIS BRDF normalized reflectance with fixed geometry (SZA: 45°; VZA: 0°), which is consistent with the processed AVHRR data (section 2.1.1), was computed with high-quality BRDF parameters in MCD43C1 from red (0.62~0.67 μm) and NIR (0.84~0.88 μm) channels (Wang et al., 2018) using semi-empirical RossThick-LiSparse reciprocal BRDF model (Roujean et al., 1992; Wanner et al., 1995; Schaaf et al., 2002) from February of 2000 to December of 2021.

2.1.3 Pseudo invariant calibration sites

To evaluate temporal consistency in spectral reflectance and vegetation index, we used a PICS, which has high temporal stability on surface optical properties (Bacour et al., 2019). In this study, a total of 26 PICS were used for cross-sensor calibration (20 sites) and validation (6 sites), which were registered in U.S. Geological Survey (USGS) radiometric sites catalog (https://calval.cr.usgs.gov/apps/radsites_catalog) and Committee on Earth Observation Satellites (CEOS) (https://calvalportal.ceos.org/) (Fig. A2; Table A2). Considering the characteristic of PICS, robust long-term data are expected to have no significant trends and less interannual variability in spectral reflectance and vegetation index (Latifovic et al., 2012; Zhang et al., 2017; Giglio and Roy, 2020).

2.2 Methods

Before applying the three-step post processing, we calculated monthly 0.05° spectral reflectance ($AVHRR_{LTDR}$) by averaging daily spectral reflectance in each pixel. To fill the remaining data gaps, we introduced a widely used harmonic analysis of time series (HANTS) method using 'HANTS' function in MATLAB (Abouali, 2023). Then we calculated monthly NDVI (Tucker, 1979) and NIRv (Badgley et al., 2017) with monthly gap-filled, BRDF normalized NIR and red reflectance.

2.2.1 Cross-sensor calibration

To mitigate the inconsistent bias in surface reflectance among different AVHRR sensors, we conducted cross-sensor calibration using a simple linear regression model. First, we extracted the monthly NIR and red reflectance in 20 calibration PICS (Table A1). We filtered out the outliers that have two standard deviations above or below the average values for each instrument, mostly caused by undetected sub pixel clouds, shadows or haze (Latifovic et al., 2012). Second, we derived the linear regression coefficients between the target spectral reflectance from each AVHRR satellite and the reference spectral reflectance from MetOP-B (Table 1). We used spectral reflectance from the latest sensor in the LTDR V5 (MetOP-B) as a reference for cross sensor-calibration which had reliable sensor characteristics and observation conditions (Santamaria-Artigas et al., 2021). We calculated the cross-calibration factor of each AVHRR satellite by averaging linear regression coefficients in 20 calibration PICS (Table A2). Last, we applied the derived cross-calibration factor of each AVHRR satellite to the original $AVHRR_{LTDR}$ spectral reflectance to generate cross-calibrated ($AVHRR_{cross\text{-}calibrated}$) spectral reflectance. Independent 6 validation PICS were used to evaluate the temporal consistency in

$AVHRR_{cross\text{-}calibrated}$ and vegetation indices. $AVHRR_{cross\text{-}calibrated}$ was calculated with the following equations:

$$\rho_{reference} = m_{i,j} \times \rho_{target} \tag{1}$$

$$CF = \frac{\sum_{1}^{20} m_{i,j}}{20} \tag{2}$$

$$AVHRR_{cross-calibrated}\ spectral\ reflectance = CF \times AVHRR_{LTDR}\ spectral\ reflectance \tag{3}$$

where i is number of PICS, j is spectral channel (red and NIR band), $\rho_{reference}$ is the reference spectral reflectance from MetOP-B and ρ_{target} is the spectral reflectance from each AVHRR satellite (Table 1). CF is cross-calibration factor of each satellite period.

2.2.2 Orbital drifting correction

To minimize orbital drift effects on AVHRR sensors, we applied a second correction to $AVHRR_{cross\text{-}calibrated}$ spectral reflectance in each pixel. First, we computed the linear model between spectral reflectance and SZA in each pixel. To avoid spurious correlations between spectral reflectance and SZA, we used detrended the annual anomalies in both spectral reflectance and SZA. Second, we calculated the orbit-correction factor by applying linear model to monthly SZA anomalies across the global pixels. Last, we calculated orbit-corrected ($AVHRR_{orbit\text{-}corrected}$) spectral reflectance by subtracting orbit-correction factor from the $AVHRR_{cross\text{-}calibrated}$ spectral reflectance. Then we evaluated the interannual variability and detrended annual anomaly in $AVHRR_{LTDR}$, $AVHRR_{cross\text{-}calibrated}$, and $AVHRR_{orbit\text{-}corrected}$ spectral reflectance and vegetation index at the PICS to assess temporal consistency. $AVHRR_{orbit\text{-}corrected}$ spectral reflectance was calculated with the following equation:

$$\Delta annual\ AVHRR_{cross-calibrated\ i} = a_i \times \Delta annual\ SZA_i + b_i \tag{4}$$

$$OCF_i = a_i \times \Delta monthly\ SZA_i + b_i \tag{5}$$

$$AVHRR_{orbit-corrected}\ spectral\ reflectance_i = AVHRR_{cross-calibrated}\ spectral\ reflectance_i - OCF_i \tag{6}$$

where i is number of global pixels, a_i is linear regression coefficient, b_i is intercept, $\Delta annual\ AVHRR_{cross-calibrated\ i}$ and $\Delta annual\ SZA_i$ are detrended annual anomalies in spectral reflectance and SZA, $\Delta monthly\ SZA_i$ is monthly anomaly in SZA, and OCF_i is orbit-correction factor.

2.2.3 Harmonization

To harmonize the $AVHRR_{orbit\text{-}corrected}$ vegetation indices with MODIS vegetation indices, we applied a two-step harmonization process. We considered the latest version of MODIS vegetation indices (Collection 6.1) as the most reliable and well-validated products (Zhang et al., 2017; Miura et al., 2021; Zhu et al., 2021). The discrepancies in sensor characteristics between AVHRR and MODIS resulted in the different responses of spectral reflectance to atmospheric and surface conditions, which led to differences in vegetation index (Chen et al., 2019; Zeng et al., 2022). To account for those differences in vegetation index, we used additional explanatory variables for considering atmospheric condition (aerosol optical depth and cloud fraction) and surface condition (snow cover and land cover type). The harmonization process consists of a pixel-wise linear model (Mao et al., 2012) and a machine learning-based approach to consider the non-linear relationship between $AVHRR_{orbit\text{-}corrected}$ and MODIS vegetation indices (Berner et al., 2020). First, we computed the linear model between the monthly $AVHRR_{orbit\text{-}corrected}$ NDVI and NIRv and MODIS NDVI and NIRv from 2000 to 2021 at the corresponding pixel and applied it to $AVHRR_{orbit\text{-}corrected}$ NDVI and NIRv. Second, we generated harmonized vegetation index ($AVHRR_{harmonized}$) by training the Cubist regression model (Quinlan, 1992) with five input variables including linearly-adjusted $AVHRR_{orbit\text{-}corrected}$ vegetation index, aerosol optical depth, cloud fraction, snow cover, and land cover type. We randomly selected training pixels in odd years and selected the validation pixels in even years from the same overlapping periods for 2000–2021. The Cubist model performed well in both the training (R^2=0.93–0.94) and validation (R^2=0.90–0.91) (Fig. A5). We used the resampled 0.05°, monthly MERRA-2 aerosol optical depth (Randles et al., 2017), ERA-5 cloud fraction, snow cover data (Hersbach et al., 2020), the MCD12C1 land cover product with the International Geosphere–Biosphere Programme (IGBP) scheme for the period 2001–2019 (Friedl and Sulla-Menashe, 2015), and the European Space Agency Climate Change Initiative (ESA-CCI) land cover product converted into IGBP classes for the period before 2001 (Defourny et al., 2012). $AVHRR_{harmonized}$ vegetation index was calculated with the following equations:

$$MODIS\ vegetation\ index_i = a_i \times \mathrm{AVHRR}_{orbit-corrected}\ vegetation\ index_i + b_i \tag{7}$$

$$Adj\ \mathrm{AVHRR}_{orbit-corrected}\ vegetation\ index_i = a_i \times \mathrm{AVHRR}_{orbit-corrected}\ vegetation\ index_i + b_i \tag{8}$$

$$\mathrm{AVHRR}_{harmonized}\ vegetation\ index_i = f(Adj\ \mathrm{AVHRR}_{orbit-corrected}, AOD, CLD, SNW, LC)_i \tag{9}$$

where i is number of global pixels, a_i is linear regression coefficient, b_i is intercept, $Adj\ \mathrm{AVHRR}_{orbit-corrected}\ vegetation\ index$ is a linearly-adjusted $\mathrm{AVHRR}_{\text{orbit-corrected}}$ vegetation index. AOD, CLD, SNW, and LC indicate aerosol optical depth, cloud fraction, snow cover, and land cover type, respectively.

2.2.4 Statistical analysis

We applied the widely used Mann-Kendall test for calculating long-term trends in vegetation index (Chen et al., 2019), a non-parametric test for detecting monotonic trends in time series data. We used the 'pyMannKendall' python function (Hussain and Mahmud, 2019). We calculated annual growing season vegetation indices by averaging monthly vegetation values with temperature climatology ≥0°C (Prentice et al., 2011). Then we computed pixel-wise growing season NDVI and NIRv trends in each period including 1982-2021, 1982-1999 and 2000-2021. For global trends, we calculated global NDVI and NIRv by calculating area-weighted averaged values.

To investigate the relative effects of cross-calibration, orbit correction, and harmonization on trends in vegetation indices, we quantified the effects of each processing on trends. We defined the effect of each processing on trends as the relative changes in trends between consecutive processing steps: $\mathrm{AVHRR}_{\text{LTDR}}$–$\mathrm{AVHRR}_{\text{cross-calibrated}}$, $\mathrm{AVHRR}_{\text{cross-calibrated}}$–$\mathrm{AVHRR}_{\text{orbit-corrected}}$, and $\mathrm{AVHRR}_{\text{orbit-corrected}}$–$\mathrm{AVHRR}_{\text{harmonized}}$.

3 Results

3.1 Evaluation of $\mathrm{AVHRR}_{\text{LTDR}}$ and $\mathrm{AVHRR}_{\text{cross-calibrated}}$ data

We found an enhanced temporal consistency in $\mathrm{AVHRR}_{\text{cross-calibrated}}$ spectral reflectances and vegetation indices compared to $\mathrm{AVHRR}_{\text{LTDR}}$ at the PICS (20 sites for calibration and 6 sites for validation) (Fig. 1). Across the PICS, AVHRR$_{LTDR}$ NIR reflectance showed a notable increasing trend, while AVHRR$_{LTDR}$ red reflectance had a decreasing trend for 1982-2021 (NIR: -0.0002±0.0003 yr^{-1}; Red:0.0003±0.0002 yr^{-1}). Both AVHRR$_{LTDR}$ NDVI and NIRv showed a clear decreasing trend (NDVI: -0.0006±0.0002 yr^{-1}; NIRv: -0.0003±0.0001 yr^{-1}). After applying cross-calibration, NIR, red reflectance, NDVI, and NIRv showed a reduced trend at both the calibration and validation PICS. The impact of cross-sensor calibration on the AVHRR-2 sensor periods (NOAA 07, 09, 11, and 14) was considerable, whereas the AVHRR-3 sensor periods (NOAA 16, 18, and 19) exhibited relatively minor differences between the original LTDR and cross-calibrated data (Fig. 1; Table A3).

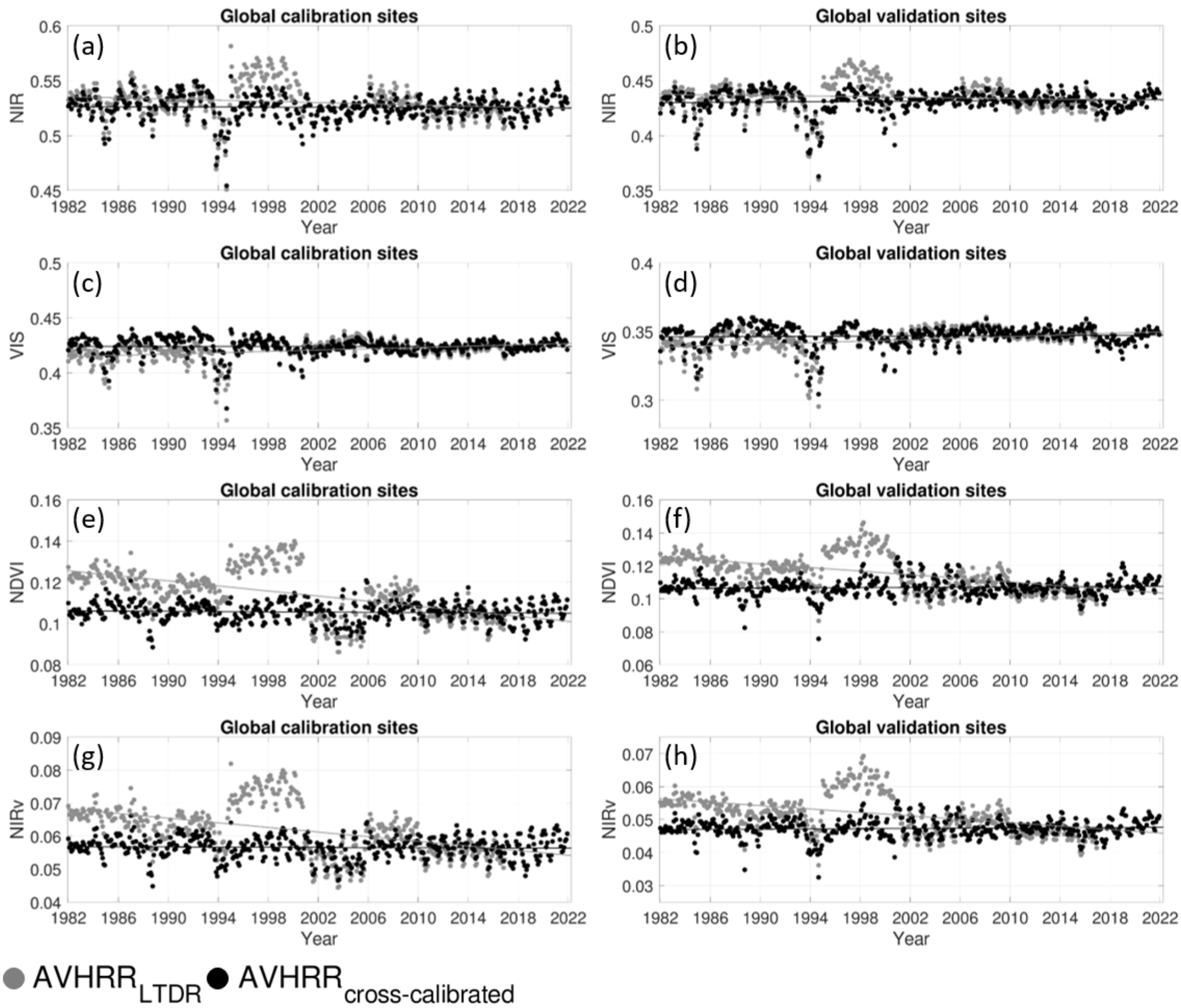

Figure 1. Comparison of averaged cross-calibrated and original LTDR AVHRR NIR (a-b), red reflectance (c-d), NDVI (e-f), and NIRv (g-h) at Pseudo-invariant Calibration Site (PICS) over 1982-2021. Total 26 PICS were used for calibration (20 sites) and validation (6 sites). Grey dots indicate original LTDR AVHRR

data and black dots indicate cross-calibrated AVHRR data.

3.2 Evaluation of $AVHRR_{cross\text{-}calibrated}$ and $AVHRR_{orbit\text{-}corrected}$ data

Our results demonstrated that orbit-drifting correction reduced the temporal inconsistency in $AVHRR_{cross\text{-}calibrated}$ spectral reflectances and vegetation indices across the PICS (Fig. 2; Fig. A4). We examined the detrended annual anomalies for each processing levels of data. $AVHRR_{LTDR}$ spectral reflectance and vegetation indices had a marked temporal inconsistency, whereas both cross-calibrated and orbit-corrected data showed improved temporal consistency throughout the 1982-2021 (Fig. 2). Both cross-sensor calibration and orbit-drifting correction led to a reduction in interannual variability for red, NIR reflectance, NDVI, and NIRv (Fig. A4; Table A3). The interannual variability of spectral reflectances decreased from original LTDR (NIR: 0.0136±0.0025; Red: 0.0086±0.0039) to cross-calibrated (NIR: 0.0091±0.0036; Red: 0.0078±0.0044) and further to orbit-corrected (NIR: 0.0083±0.0036; Red: 0.0071±0.0045) data. NDVI and NIRv also showed a reduced interannual variability in cross-calibrated (NDVI: 0.0057±0.0025; NIRv: 0.0029±0.0009) and orbit-corrected (NDVI: 0.0055±0.0020; NIRv: 0.0027±0.0007) data compared to the LTDR NDVI and NIRv (NDVI: 0.0090±0.0027; NIRv: 0.0056±0.0012). Furthermore, we confirmed that the orbit-drifting effect was strong when the SZA remarkably changed, especially in 1994 (Fig. 2).

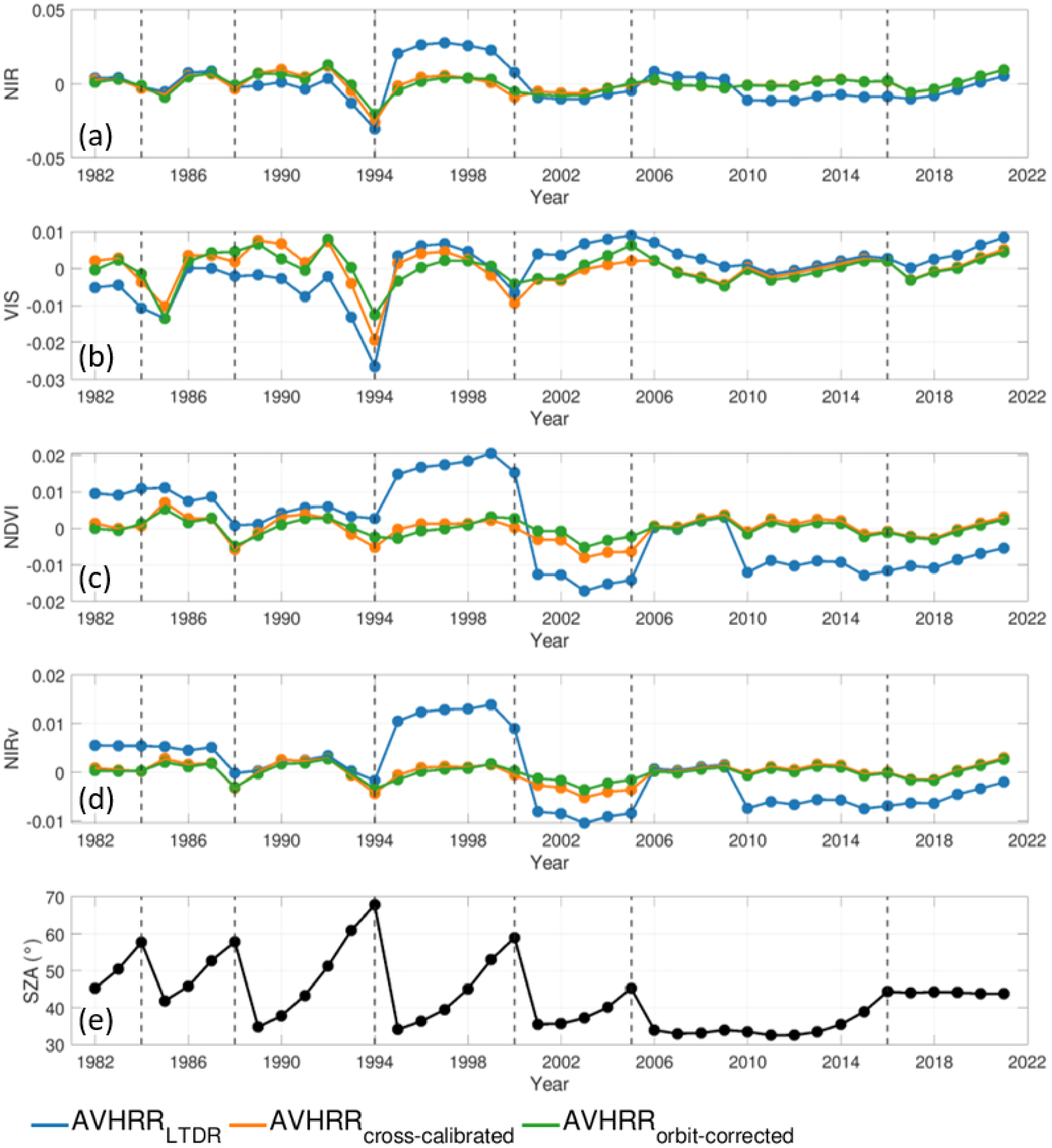

Figure 2 Comparison of detrended anomalies in original LTDR, cross-calibrated, and orbit-corrected AVHRR spectral reflectances (a-b) and vegetation indices (c-d) at Pseudo-invariant Calibration Site (PICS) sites over 1982-2021. Blue dotted lines are LTDR, orange dotted lines are cross-calibrated, and green dotted lines are orbit-corrected annual averaged AVHRR data, respectively. Black dotted lines indicate the annual averaged solar zenith angle at PICS.

3.3 Evaluation of AVHRR$_{orbit\text{-}corrected}$ and AVHRR$_{harmonized}$ data

We found that harmonization with MODIS also effectively reduced the residual temporal inconsistency in $\mathrm{AVHRR}_{\mathrm{orbit\text{-}corrected}}$ vegetation indices (Fig. 3). Our results showed a less interannual variability and trend in $\mathrm{AVHRR}_{\mathrm{harmonized}}$ vegetation indices compared to $\mathrm{AVHRR}_{\mathrm{orbit\text{-}corrected}}$ vegetation indices (Fig. 3). Both $\mathrm{AVHRR}_{\mathrm{harmonized}}$ NDVI and NIRv showed a strong temporal relationship with MODIS NDVI and NIRv during the overlapping period (Fig. 4). The $\mathrm{AVHRR}_{\mathrm{harmonized}}$ NDVI and NIRv showed a consistent seasonal pattern with MODIS NDVI and NIRv across latitudes (Fig. 5). The spatial distribution of $\mathrm{AVHRR}_{\mathrm{harmonized}}$ NDVI and NIRv trends also well matched with MODIS during the overlapping period (Fig. 6; NDVI: 89.3%; NIRv: 89.5%). Furthermore, we found that the disagreed trend pixels between $\mathrm{AVHRR}_{\mathrm{harmonized}}$ and MODIS vegetation indices were distributed sparsely rather than appearing in a specific region or ecosystem.

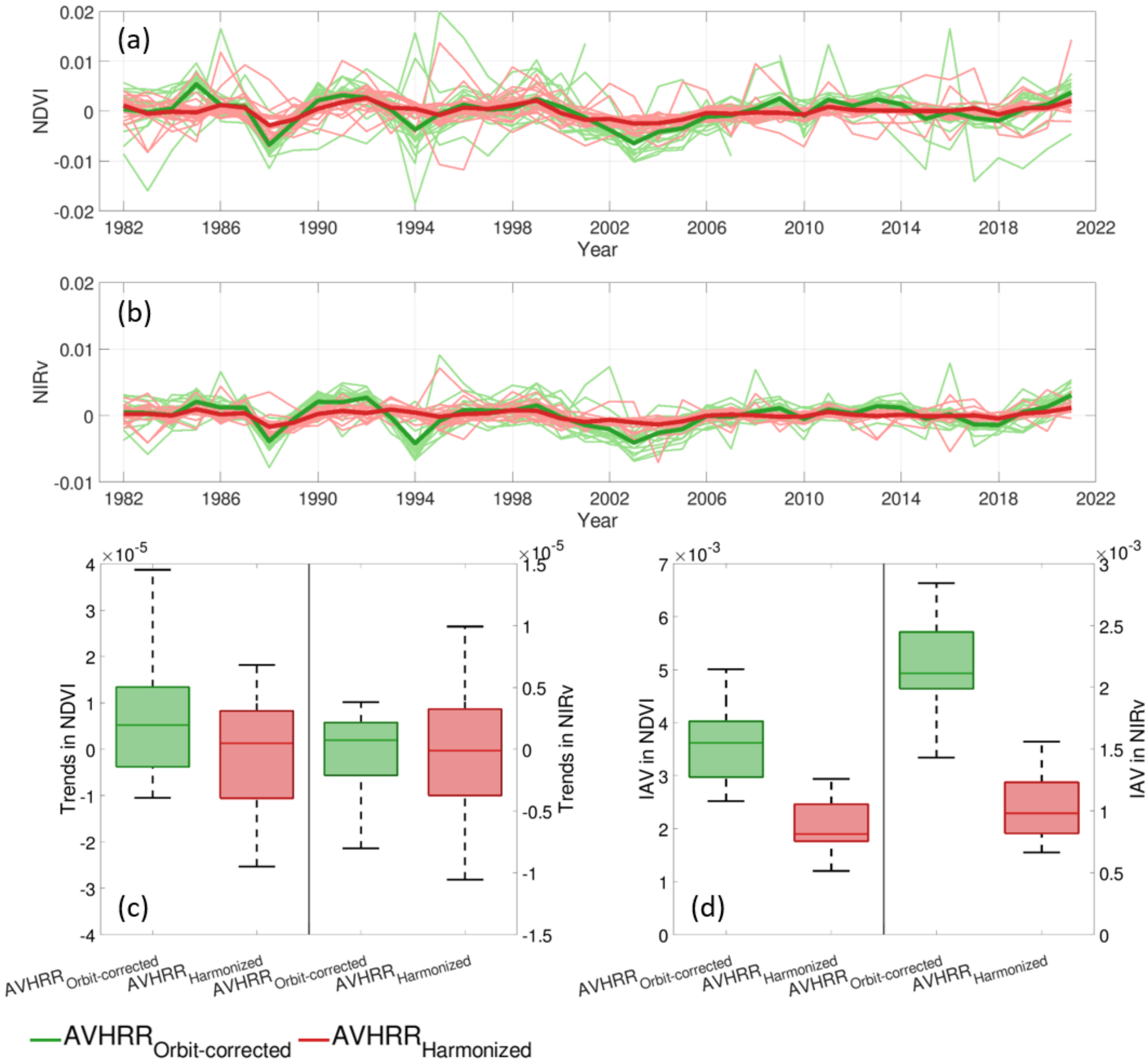

Figure 3 Comparison of detrended anomalies (a-b), trends (c), and interannual variability (d) in orbit-corrected AVHRR and harmonized AVHRR data at Pseudo-invariant Calibration Site (PICS) sites over 1982-2021. Thick lines in (a) and (b) are averaged detrended anomalies. The different colors represent orbit-corrected (green) and harmonized (red), respectively.

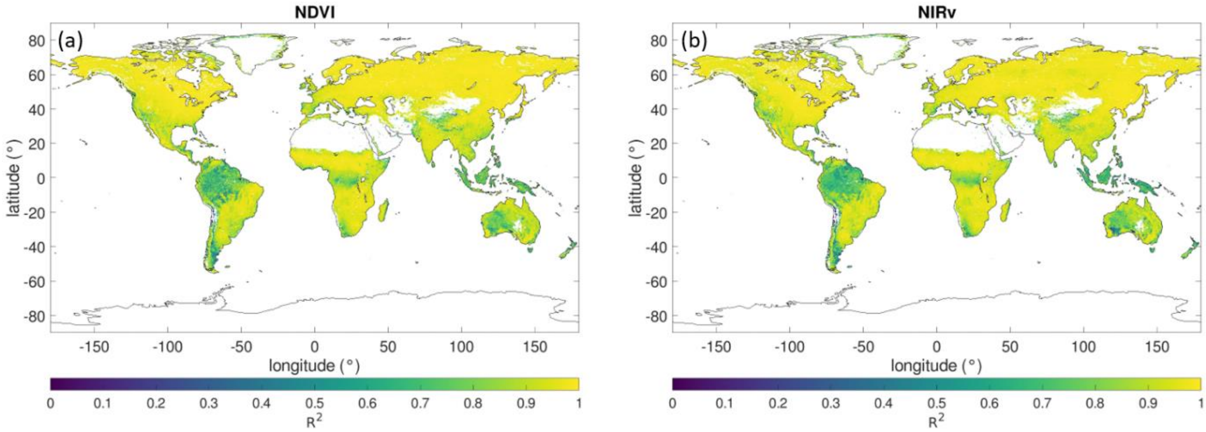

Figure 4 Spatial distribution of coefficient of determination (R^2) between monthly harmonized AVHRR and MODIS NDVI (a) and NIRv (b) for 2000-2021.

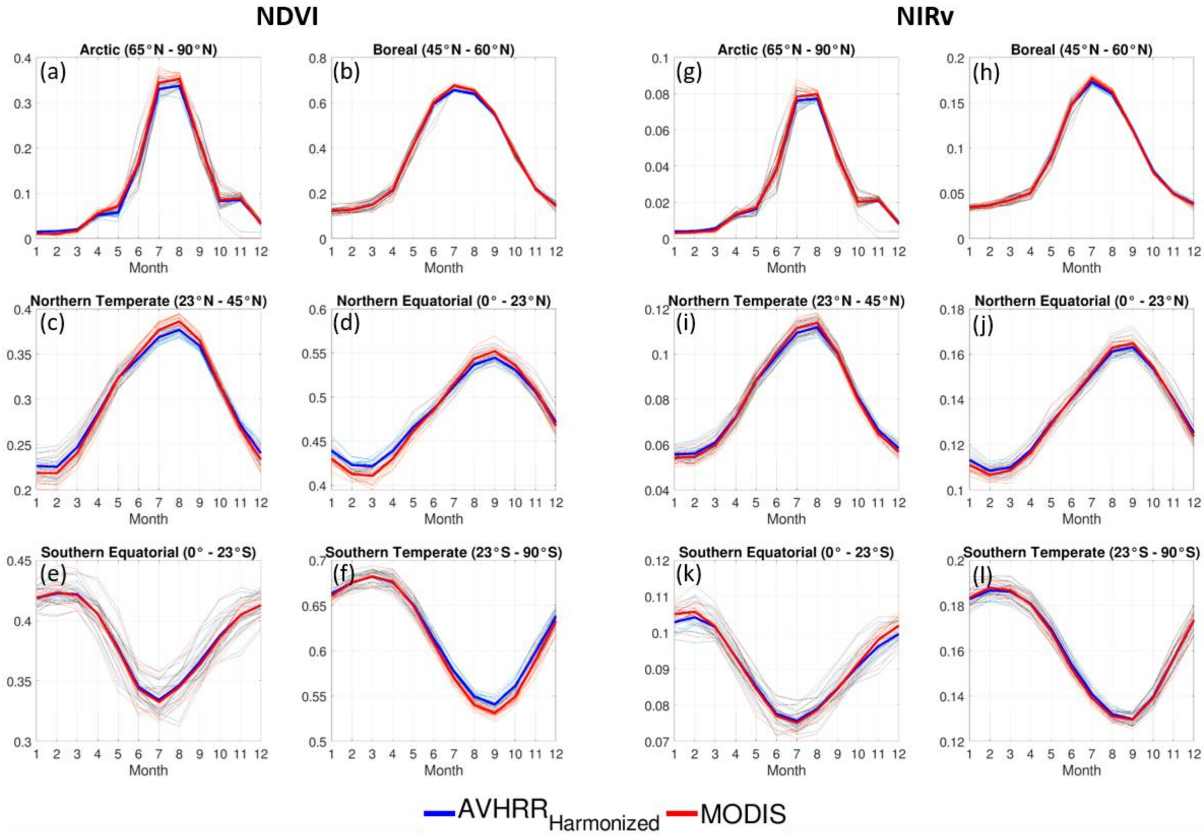

Figure 5 Comparison of seasonal pattern between harmonized AVHRR (Blue) (a-f) and MODIS (Red) (g-l) NDVI and NIRv. The thin lines indicate a seasonal pattern in each year for 2000-2021 and the thick lines indicate an averaged seasonal pattern.

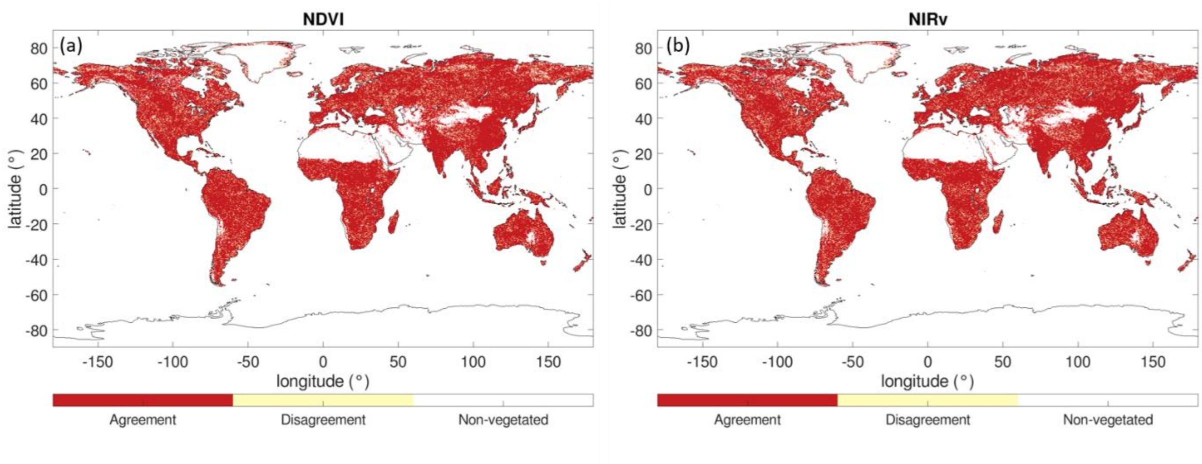

Figure 6 Spatial distribution of agreements between harmonized AVHRR and MODIS NDVI (a) and NIRv (b) for 2000-2021. Red, yellow, and white color indicate agreement, disagreement, and non-vegetated pixels, respectively.

3.4 Comparison of NDVI and NIRv trends with different processing levels

We found that the global long-term trends in NDVI and NIRv with four different processing levels differed considerably. First, we examined the long-term trends in NDVI and NIRv using four different processing levels from 1982 to 2021 (Fig. 7). All of NDVI and NIRv in different processing levels showed significant increasing trend. The original $\mathrm{AVHRR}_{\mathrm{LTDR}}$ had similar trends with $\mathrm{AVHRR}_{\mathrm{harmonized}}$, but the interannual variability of $\mathrm{AVHRR}_{\mathrm{LTDR}}$ had three times larger in NDVI and four times larger in NIRv than $\mathrm{AVHRR}_{\mathrm{harmonized}}$. The interannual variability in NDVI and NIRv were gradually reduced as we conducted each processing. Second, we investigated the trends in 1982-1999 and 2000-2021 separately to compare the effect of each processing further (Fig. 8). Compared to $\mathrm{AVHRR}_{\mathrm{harmonized}}$, $\mathrm{AVHRR}_{\mathrm{LTDR}}$ NDVI and NIRv showed stronger greening trends during 1982-1999 (NDVI: $\mathrm{AVHRR}_{\mathrm{LTDR}}$: 0.0017 y^{-1}; $\mathrm{AVHRR}_{\mathrm{harmonized}}$: 0.0008 y^{-1}; NIRv: $\mathrm{AVHRR}_{\mathrm{LTDR}}$: 0.0008 y^{-1}; $\mathrm{AVHRR}_{\mathrm{harmonized}}$: 0.0003 y^{-1}), while the $\mathrm{AVHRR}_{\mathrm{LTDR}}$ NDVI and NIRv exhibited a weakened greening trend during 2000-2021 (NDVI: $\mathrm{AVHRR}_{\mathrm{LTDR}}$: 0.0005 y^{-1}; $\mathrm{AVHRR}_{\mathrm{harmonized}}$: 0.0008 y^{-1}; NIRv: $\mathrm{AVHRR}_{\mathrm{LTDR}}$: 0.0001 y^{-1}; $\mathrm{AVHRR}_{\mathrm{harmonized}}$: 0.0003 y^{-1}). The proportion of statistically significant greening trend pixels ($p < 0.1$) increased as the processing progressed from $\mathrm{AVHRR}_{\mathrm{LTDR}}$, $\mathrm{AVHRR}_{\mathrm{cross\text{-}calibrated}}$, and $\mathrm{AVHRR}_{\mathrm{orbit\text{-}corrected}}$ to $\mathrm{AVHRR}_{\mathrm{harmonized}}$ for 1982-1999, while the proportion of significantly greening trend pixels decreased as the processing progressed for 2000-2021 in both NDVI and NIRv (Fig. A6; Table A5).

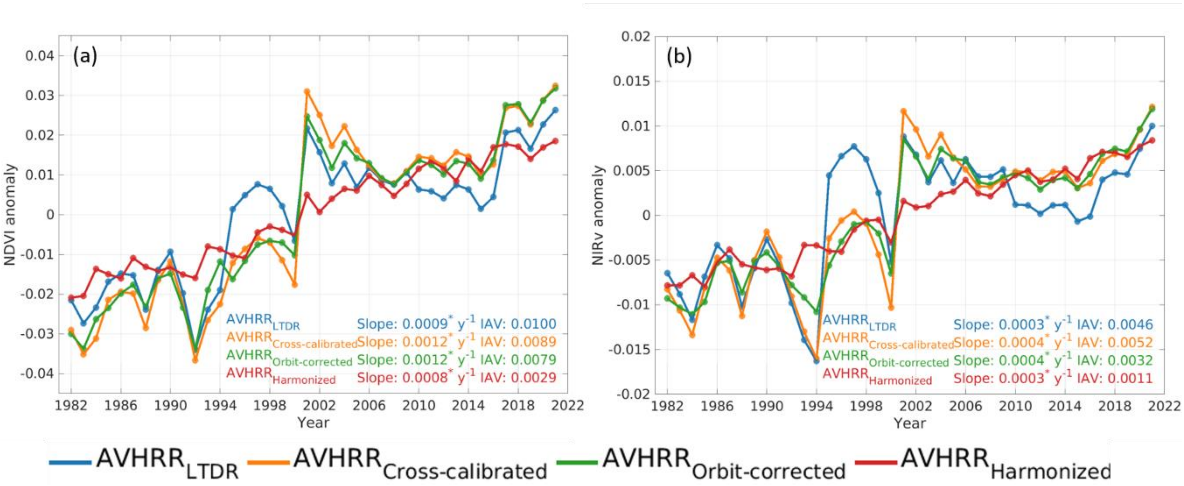

Figure 7 Temporal dynamics in global long-term AVHRR NDVI (a) and NIRv (b) with different processing levels. The different colors represent original LTDR (blue), cross-calibrated (orange), orbit-corrected (green), and harmonized (red) NDVI and NIRv, respectively

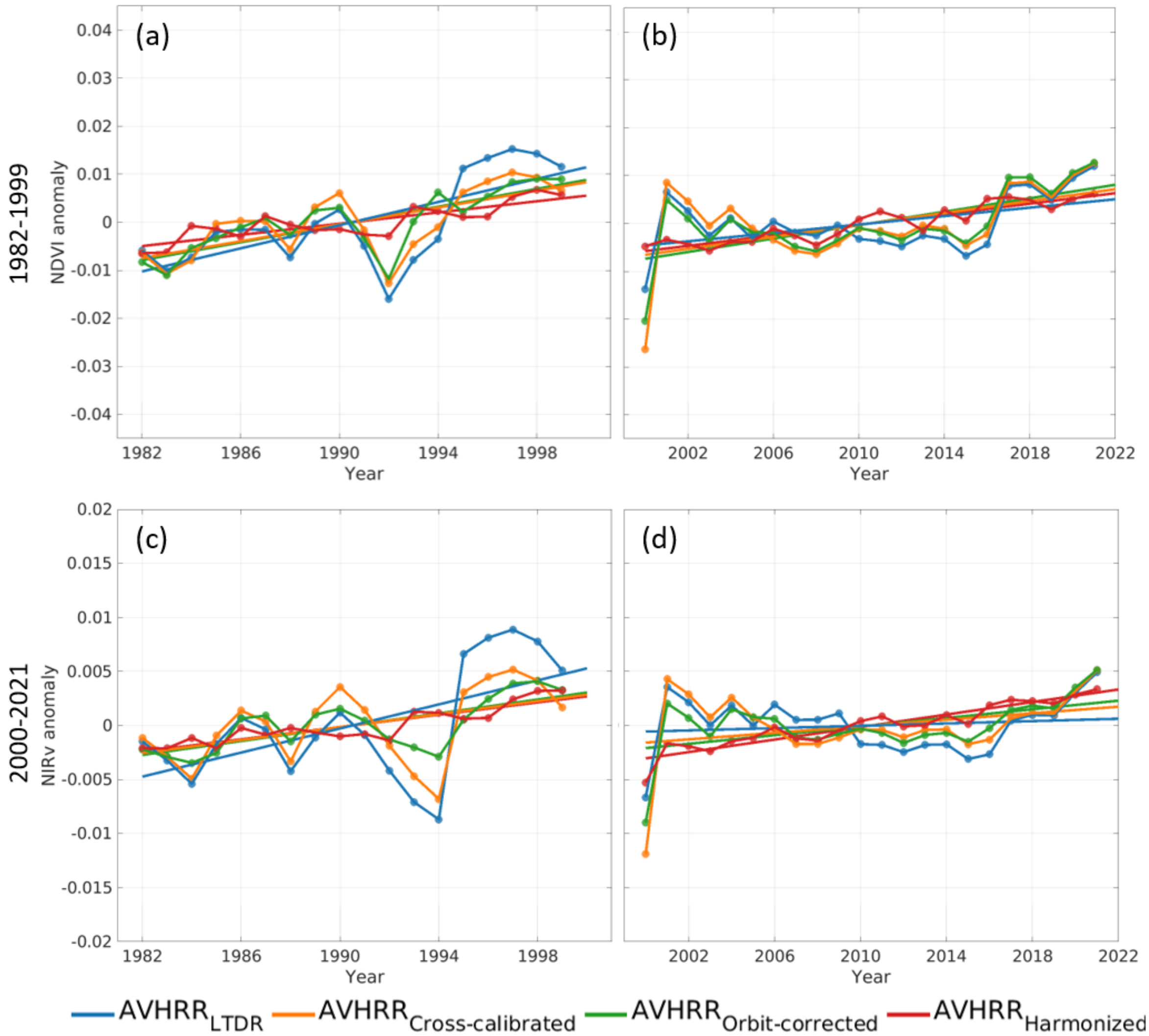

Figure 8 Annual anomalies in different processing levels of long-term AVHRR NDVI (a-b) and NIRv (c-d) for 1982-1999 and 2000-2021. The different colors represent original LTDR (blue), cross-calibrated (orange), orbit-corrected (green), and harmonized (red) NDVI and NIRv, respectively

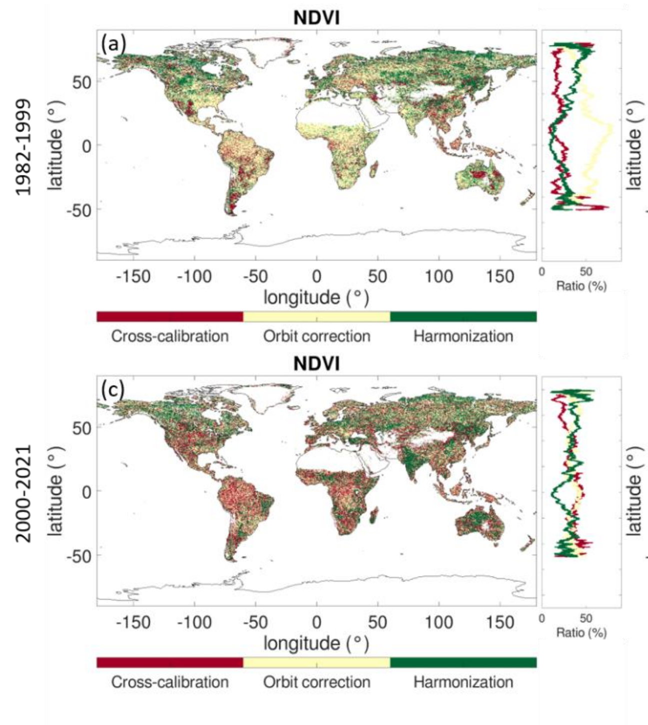

Figure 9 Comparison of the relative three processing effects on long-term trends in NDVI and NIRv for 1982-1999 and 2000-2021. The largest effects of processing were marked followed colors: cross-calibration (red), orbit correction (yellow), and harmonization (green).

We found that the relative effects of cross-calibration, orbit correction, and harmonization on trends in vegetation indices were different for earlier AVHRR satellites (1982-1999) and later AVHRR satellites (2000-2021) (Fig. 9). Over the period from 1982 to 1999, the orbital drifting correction had a dominant impact on the long-term vegetation index trends particularly around the equator (NDVI: Cross-calibration: 19.1%; Orbit correction: 53.2%; Harmonization: 27.7%; NIRv: Cross-calibration: 12.9%; Orbit correction: 57.3%; Harmonization: 29.8%). Orbit correction had a notable effect near the equator, where a larger SZA anomaly was observed compared to other regions (Fig. A3). The harmonization also showed a considerable effect on long-term trends in NDVI and NIRv, especially in the northern hemisphere. For 2000-2021, relative effects of cross-calibration, orbit correction, and harmonization on global long-term trends in NDVI (Cross-calibration: 35.6%; Orbit correction: 31.3%; Harmonization: 33.1%) and NIRv (Cross-calibration: 35.7%; Orbit correction: 30.9%; Harmonization: 33.4%) exhibited comparable ratios. Compared by latitude, harmonization had a relatively greater impact on both NDVI and NIRv than the other two processings in the high-latitude regions.

4 Discussions

4.1 Addressing temporal inconsistency in the long-term AVHRR dataset

Our findings demonstrated that the cross-calibration can correct the inconsistent bias in spectral reflectance and vegetation index between AVHRR sensors at PICS (Fig. 1). We found that sensor cross-calibration well reduced the temporal inconsistency at a particular satellite period, such as NOAA 14 periods which were reported to have a higher bias of NIR reflectance compared to other NOAA satellite periods (Santamaria-Artigas et al., 2021; Frankenberg et al., 2021). Furthermore, we found a noteworthy decreasing trend in $AVHRR_{LTDR}$ NDVI and NIRv at PICS, which were attributed to the decreased trend in NIR reflectance and an increased trend in red reflectance (Fig. 1). After applying cross-calibration to $AVHRR_{LTDR}$ spectral reflectances, significant trends were removed in both $AVHRR_{LTDR}$ spectral reflectances and vegetation indices. In the previous study, Latifovic et al. (2012) reported cross-calibration can address temporal inconsistency in BRDF normalized reflectances from NOAA 07 to NOAA 19 at eight PICS. Li et al. (2014) also reported the improved temporal consistency of AVHRR top of atmosphere reflectance after cross-sensor calibration. Our results highlighted the robustness of the sensor cross-calibration approach in reducing temporal inconsistency over an extended validation period and a larger number of PICS (Table A1; Table A2).

Our results highlighted the significance of orbital drifting correction for decreasing interannual variability artefacts in spectral reflectances and vegetation indices (Fig. 2; Fig. A4). We found the strongly improved temporal consistency in 1994, which showed the largest anomaly in $AVHRR_{LTDR}$ and $AVHRR_{cross\text{-}calibrated}$ data across the PICS and global scale due to the largest SZA anomaly (Fig. 2; Fig. 7). These findings can help to enhance our understanding of the interannual variation in NDVI and NIRv by reducing the artefacts from orbital drifting. We also found that the orbital drifting effects on NIRv were doubled compared to NDVI (NDVI: -3.5%; NIRv: -6.9%) at PICS (Fig. A4). The higher sensitivity of NIRv to the angular effects owing to the NIR reflectance can explain the larger orbital drifting effects (Zeng et al., 2022; Jeong et al., 2023).

We further demonstrated the importance of minimizing the temporal inconsistency in $AVHRR_{orbit\text{-}corrected}$ NDVI and NIRv through the harmonization with MODIS. The reduced trends and interannual variability in $AVHRR_{harmonized}$ vegetation index at PICS underscored the improved capability of capturing vegetation signals better with harmonization (Fig. 3). In particular, $AVHRR_{harmonized}$ did not show a biased spatial agreement with MODIS vegetation indices trends across the latitudes (Fig. 6), which can support the robustness of two-step harmonization approach (Berner et al., 2020). In addition, $AVHRR_{harmonized}$ vegetation index showed a similar interannual variability with MODIS at the global scale (Fig. A8). It is contrasting with recent studies, which showed significant differences in interannual variability after applying a cumulative distribution frequency matching approach (Zhu et al., 2021; Wang et al., 2021). These findings improve the reliability of trends and interannual variability in the $AVHRR_{harmonized}$ vegetation index datasets.

4.2 Global trends in vegetation index with enhanced temporal consistency

Our results revealed a persistent greening trend in $AVHRR_{harmonized}$ NDVI and NIRv for 1982–2021. This is notably different from the previous studies which showed rapid greening trends in NIRv before 2000 followed by a relatively weakened trend after 2000 (Wang et al., 2020; Zhu et al., 2021). These discrepancies in vegetation index trends were largely due to the unresolved temporal inconsistencies in earlier datasets which led to the overestimated greening trend before 2000 and underestimated greening trend after 2000.

We suspected that the global greening trend in NDVI and NIRv can be overestimated for 1982-1999. First, we found that inconsistent bias between AVHRR sensors in $AVHRR_{LTDR}$ NDVI and NIRv can lead an overestimation of global greening trend for 1982-1999 (Fig. 1; Fig. 8). We found the primary source of an overestimated global greening trend before 2000 with the high bias in the NOAA 14 satellite LTDR NIR reflectance (Fig. 8). The strong greening $AVHRR_{LTDR}$ NIRv trend before 2000 was consistent with a recent study (Wang et al., 2020; Zhu et al., 2021) which used NIRv derived from GIMMS3g NDVI and LTDR V5 NIR reflectance. As GIMMS3g NDVI did not show a noticeable higher global NDVI anomaly during NOAA 14 periods (Tian et al., 2015), we assumed $AVHRR_{LTDR}$ NIR reflectance led greening NIRv trend before 2000. We also found orbit drifting effects can induce the overestimation of NDVI and NIRv trends for 1982-1999. Following the latitudinal gradient of

SZA changes (Fig. A3), orbit correction also showed stronger effects on trends in vegetation indices near the equator (Fig. 9). Similarly, a recent study reported severe orbital drifting effects on GIMMS3g NDVI in tropical evergreen broadleaf forest regions near the equator before 2000 (Li et al., 2023). They reported negative bias in NOAA 9 NDVI and positive bias in NOAA 11 and 14 NDVI which can cause of overestimation of the greening trend in NDVI before 2000. We found that after addressing temporal inconsistency in NDVI datasets, Amazon evergreen broadleaf forests did not show such a strong greening trend and interannual variation for 1982-1999 (Fig. A9). It is noteworthy that tropical evergreen broadleaf forests contributed the most to the uncertainty of global vegetation trends (Wang et al., 2022). In light of this, PKU GIMMS NDVI also showed a much-reduced global greening trend and interannual variation before 2000 compared to GIMMS3g NDVI (Li et al., 2023). A reduced greening trend with enhanced temporal consistency in both refined NDVI products supported our suspicion about an overestimated greening trend in 1982-1999. Therefore, future studies need to investigate the greening or browning trends and interannual variability further and their drivers during 1980-1990s using novel datasets with enhanced temporal consistency.

In contrast to 1982-1999, the global greening trend in NDVI and NIRv can be underestimated after 2000. Overall, we found that sharply declined $AVHRR_{LTDR}$ NDVI and NIRv early 2000s largely impact on trends after 2000 which was gradually increased by conducting each processing step. First, we found a considerable inconsistent bias in $AVHRR_{LTDR}$ NDVI and NIRv early 2000s. We can expect larger calibration effects in the before 2000 considering AVHRR-2 sensors often suffered from sensor degradation while AVHRR-3 sensors had a relatively stable performance (Los et al., 1998; Bhatt et al., 2016; Chen et al., 2019). But we found that NOAA 16 and 18 also had a substantial inconsistent bias in NDVI and NIRv (Fig. 1), and it makes considerable cross-calibration effects on NDVI and NIRv trends compared to orbit correction and harmonization during 2000-2021 (Fig. 9). Second, orbital drifting effects can lead to an underestimation of greening trend in vegetation index. At the global scale, orbit correction led to considerable increasing greening trend in NDVI and NIRv for 2000-2021 (Fig. 8; Table A4). This result is consistent with recent findings. While GIMMS3g showed a weak global greening trend after 2000, PKU GIMMS NDVI showed a strong global trend (Li et al., 2023). Last, AVHRR-MODIS harmonization notably affected NDVI and NIRv trends in the high-latitude regions after 2000. We may explain the higher harmonization effect in the high-latitude regions related to the difference in spectral resolution of the NIR band between AVHRR and MODIS (Fig. A1). The narrow MODIS NIR band can tightly focus on vegetation reflectance. On the other hand, broad AVHRR NIR band can dilute the signal from increasing vegetation fraction due to the larger water vapor absorption and soil interference (Gitelson et al., 1998; Van Leeuwen et al., 2006; Brown et al., 2006). Furthermore, we found a consistent greening trend between $\text{AVHRR}_{\text{harmonized}}$ and high spatial resolution Landsat NDVI at those high-latitude regions after 2000 (Berner et al., 2020; Fig. A7). As a result, addressing ongoing challenges of temporal inconsistency led to an increased global greening trend after 2000 in both refined $\text{AVHRR}_{\text{harmonized}}$ and PKU GIMMS NDVI products compared to their original products. Those findings emphasized the significance of addressing technical issues in the long-term vegetation index datasets to improve the reliability of trend analysis.

4.3 Implications for future studies

Potential users of this dataset need to consider the assumption of our long-term NDVI and NIRv data production. Basically, intrinsic differences of wavelength characteristics, sensor calibration, orbit maintenance between AVHRR and MODIS had a substantial impact on vegetation index values and trends (Chen et al., 2019; Zeng et al., 2022). This study used MODIS Collection 6.1 as a validated benchmark dataset for generating long-term NDVI and NIRv. But further improvements in the benchmark datasets could lead to a difference in long-term trends. For example, Zhang et al. (2017) reported a significant global browning trend in MODIS Collection 5 due to the sensor degradation while MODIS Collection 6 vegetation indices, which fixed the sensor degradation issue, showed greening trend. Furthermore, MODIS Terra and Aqua close to be decommissioned with orbital drifting (https://terra.nasa.gov/about/terras-orbit-changes). Future studies need to consider incorporating VIIRS in our proposed approach for generating a long-term vegetation index, while MODIS-VIIRS calibration also should be applied carefully (Fan et al., 2016).

5 Summary and Conclusion

We demonstrated an enhanced temporal consistency in the refined long-term NDVI and NIRv after applying three-step post processing including cross sensor-calibration between AVHRR sensors, orbital drifting correction among AVHRR sensors, and machine-learning based harmonization with MODIS. Our refined NDVI and NIRv dataset identified a persistent global greening trend over the last four decades. This finding is in contrast to the original LTDR V5 NDVI and NIRv, which exhibited strong greening trends prior to 2000 and diminished greening trends after 2000 stemming from the temporal inconsistency. Overall, our results highlight the critical need for reducing temporal inconsistency within vegetation index datasets and its substantial impact on long-term trends. We believe that these findings can strengthen our understanding of global long-term vegetation dynamics.

Acknowledgement

We extend our gratitude to the NASA LTDR team for providing the LTDR V5 products, the MODIS team for the MODIS BRDF products, and the GIMMS team for sharing the GIMMS3g NDVI dataset. This study was supported by National Research Foundation of Korea (NRF-2019R1A2C2084626) and by the LEMONTREE (Land Ecosystem Models based On New Theory, obseRvations and ExperimEnts) project, funded through the generosity of Eric and Wendy Schmidt by recommendation of the Schmidt Futures program.

Appendix

Table A 1 List of Pseudo Invariant Calibration Site (PICS)

Name	Latitude	Longitude
Arabia 2	20.19°	51.63°
Sudan 1	22.11°	28.11°
Arabia 1	19.80°	47.07°
Egypt 1	26.61°	26.22°
Libya 3	23.22°	23.23°
Libya 2	25.08°	20.77°
Algeria 3	30.63°	7.83°
Mauritania 1	19.51°	-8.57°
Mali 1	19.14°	-5.77°
Libya 4	28.67°	23.42°
Niger 1	20.26°	9.64°
Algeria 1	23.83°	-0.76°
Mauritania 2	19.78°	-8.89°
Algeria 4	29.99°	5.10°
Libya 1	24.65°	13.25°
Algeria 5	31.16°	2.24°
Algeria 2	25.99°	-0.62°
Niger 2	21.33°	10.60°
Niger 3	21.51°	7.86°
Arabia 3	28.80°	43.05°
Taklamakan Desert	39.83°	80.17°
Railroad Valley Playa	38.50°	115.69°
Sonoran Desert	32.35°	114.65°
Dunhuang	40.13°	94.34°

Namib Desert 1	-24.98°	15.27°
Namib Desert 2	-17.33°	12.05°

Table A 2 Mean linear regression coefficients between the target spectral reflectance in each AVHRR satellite period and reference spectral reflectance from MetOP-B at the 20 calibration PICS

Satellite	**Slope**		**R^2**	
	Red-band	NIR-band	Red -band	NIR-band
NOAA-07	1.021	0.990	0.974	0.970
NOAA-09	1.011	0.989	0.950	0.968
NOAA-11	1.015	0.996	0.988	0.961
NOAA-14	0.998	0.953	0.977	0.985
NOAA-16	0.996	1.009	0.949	0.980
NOAA-18	0.992	0.981	0.921	0.985
NOAA-19	1.001	1.011	0.987	0.990

Table A 3 Interannual variability at PICS

Name	**LTDR**	**Cross-calibrated**	**Orbit-corrected**
NIR reflectance	0.0136±0.0025	0.0091±0.0036	0.0083±0.0036
Red reflectance	0.0086±0.0039	0.0078±0.0044	0.0071±0.0045
NDVI	0.0090±0.0027	0.0057±0.0025	0.0055±0.0020
NIRv	0.0056±0.0012	0.0029±0.0009	0.0027±0.0007

Table A 4 Proportion of greening and browning trend pixels in each processing levels of NDVI and NIRv for three different periods. Values in parenthesis indicate the proportion of statistically significant trend pixels.

		1982-1999		**2000-2021**		**1982-2021**	
		NDVI	**NIRv**	**NDVI**	**NIRv**	**NDVI**	**NIRv**
Greening	LTDR	85.23%	88.67%	56.27%	44.69%	82.46%	77.33%

		(35.49%)	(37.36%)	(20.36%)	(13.69%)	(61.35%)	(51.97%)
	Cross-calibrated	77.57% (29.49%)	76.70% (28.31%)	60.08% (22.66%)	52.60% (18.10%)	92.71% (77.06%)	89.70% (70.17%)
	Orbit-corrected	77.62% (27.37%)	76.91% (24.40%)	63.89% (25.65%)	58.67% (24.00%)	89.97% (74.87%)	87.74% (70.15%)
	Harmonized	71.31% (19.58%)	75.82% (24.54%)	73.24% (32.10%)	75.62% (35.64%)	86.55% (66.71%)	86.53% (70.37%)
		NDVI	**NIRv**	**NDVI**	**NIRv**	**NDVI**	**NIRv**
Browning	LTDR	14.77% (1.02%)	11.33% (1.00%)	43.73% (12.95%)	55.31% (20.65%)	17.54% (5.39%)	22.67% (7.12%)
	Cross-calibrated	22.43% (1.94%)	23.30% (2.28%)	39.92% (10.59%)	47.40% (15.31%)	7.29% (1.70%)	10.30% (2.57%)
	Orbit-corrected	22.38% (2.06%)	23.09% (2.40%)	36.11% (10.10%)	41.33% (13.57%)	10.03% (3.73%)	12.26% (4.43%)
	Harmonized	28.69% (2.39%)	24.18% (1.91%)	26.76% (5.28%)	24.38% (3.98%)	13.45% (4.37%)	13.47% (5.57%)

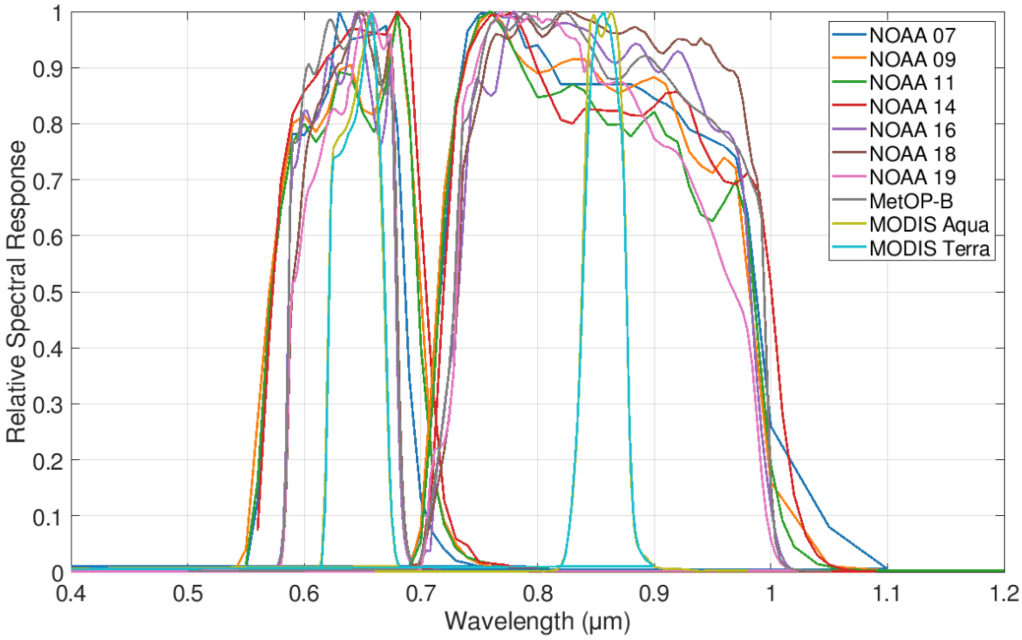

Figure A 1 Relative spectral response from AVHRR satellites and MODIS obtained from https://cloudsway2.larc.nasa.gov.

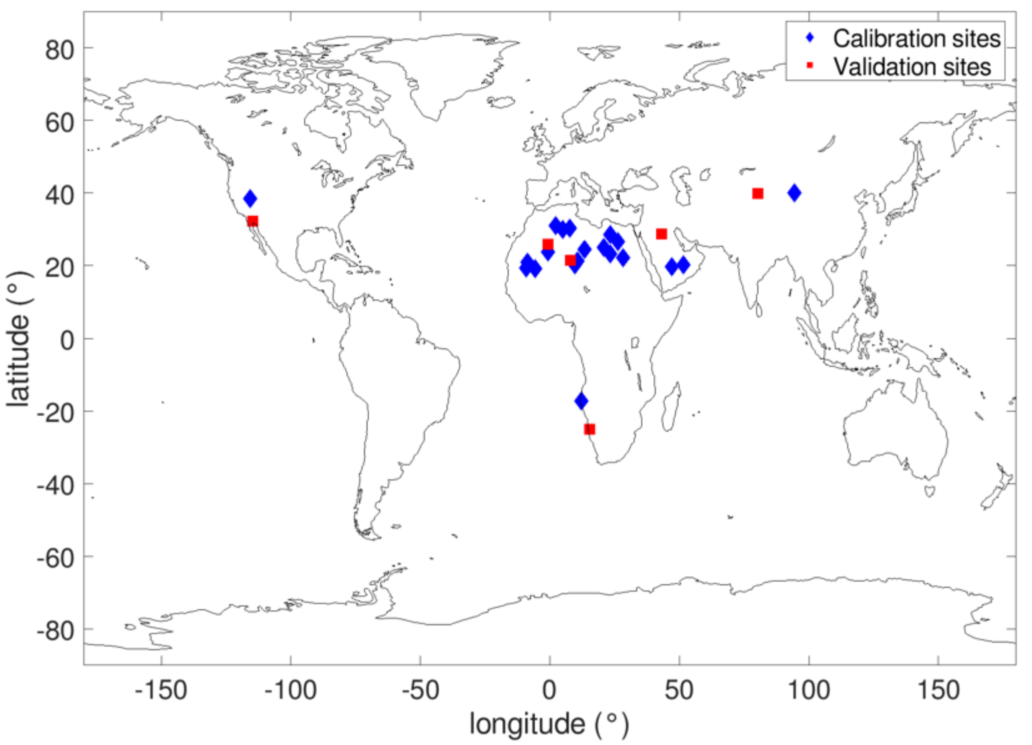

Figure A 2 Global distribution of Pseudo-invariant Calibration Site (PICS) used for calibration and validation of AVHRR time series. Total 26 PICS were used for calibration (20 sites) and validation (6 sites).

Blue diamond indicates calibration sites, and red square indicate validation sites.

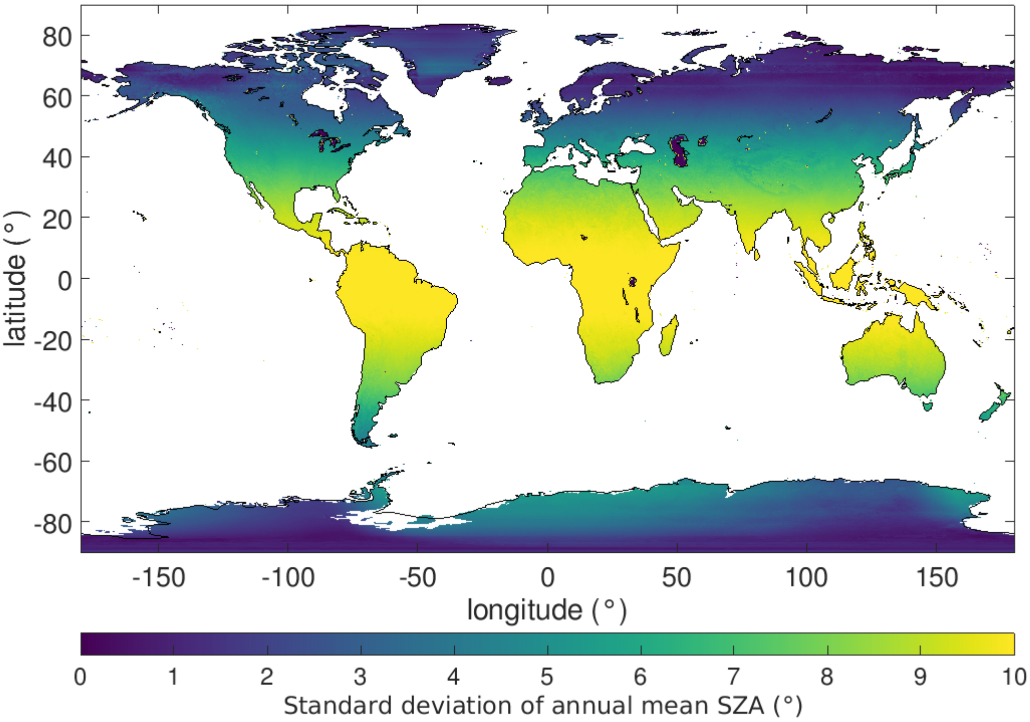

Figure A 3 Standard deviation of annual mean solar zenith angle at overpass time in each pixel from 1982 to 2021.

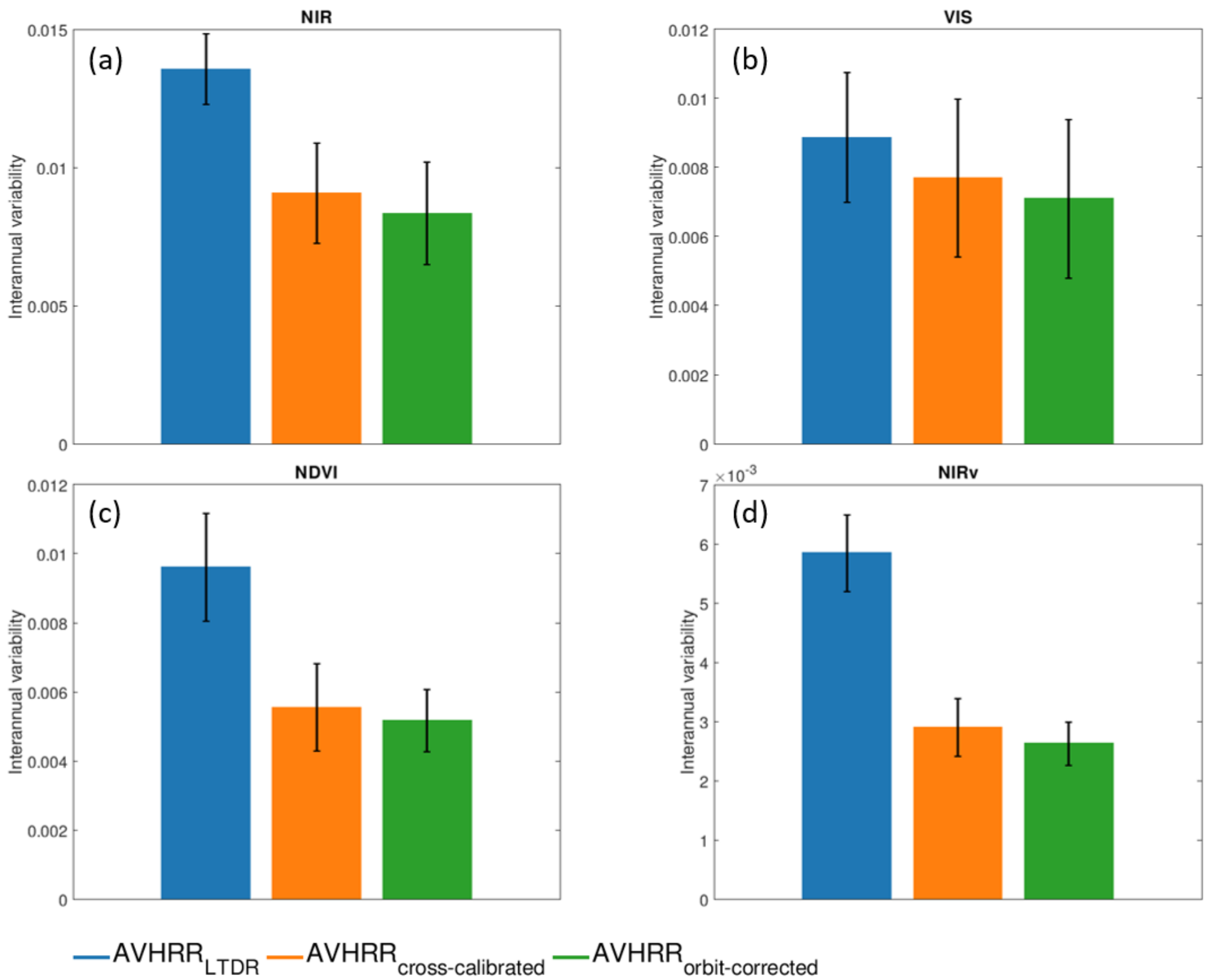

Figure A 4 Interannual variability of NIR, Red reflectance, NDVI, and NIRv for 1982-2021 at 26 Pseudo-invariant Calibration Site (PICS). The different colors represent LTDR (blue), cross-calibrated (orange), and orbit-corrected (green) respectively. Black error bars indicate the standard deviation of each interannual variability in each processing level of data.

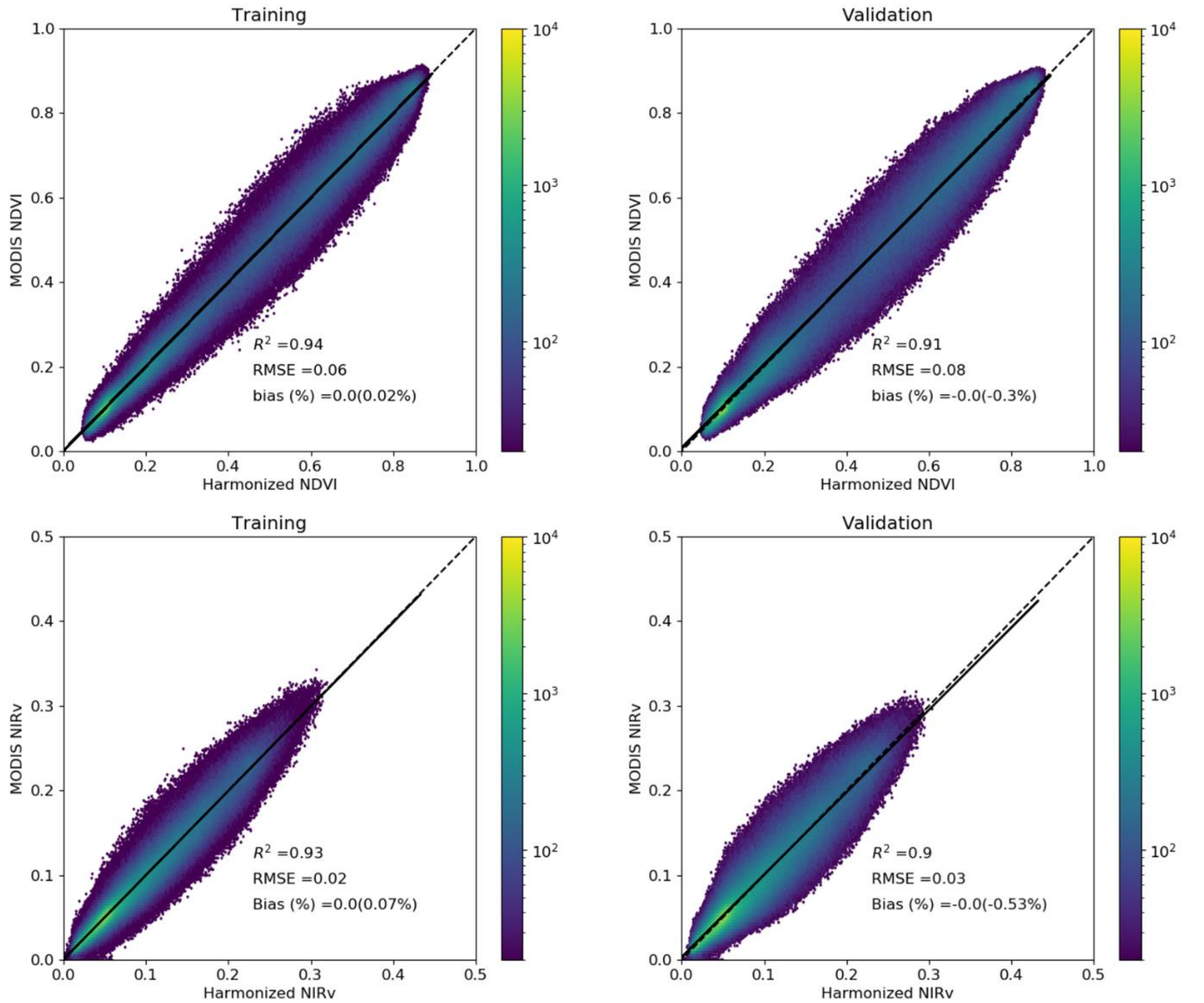

Figure A 5 The performance of the Cubist model for NDVI and NIRv in training and validation.

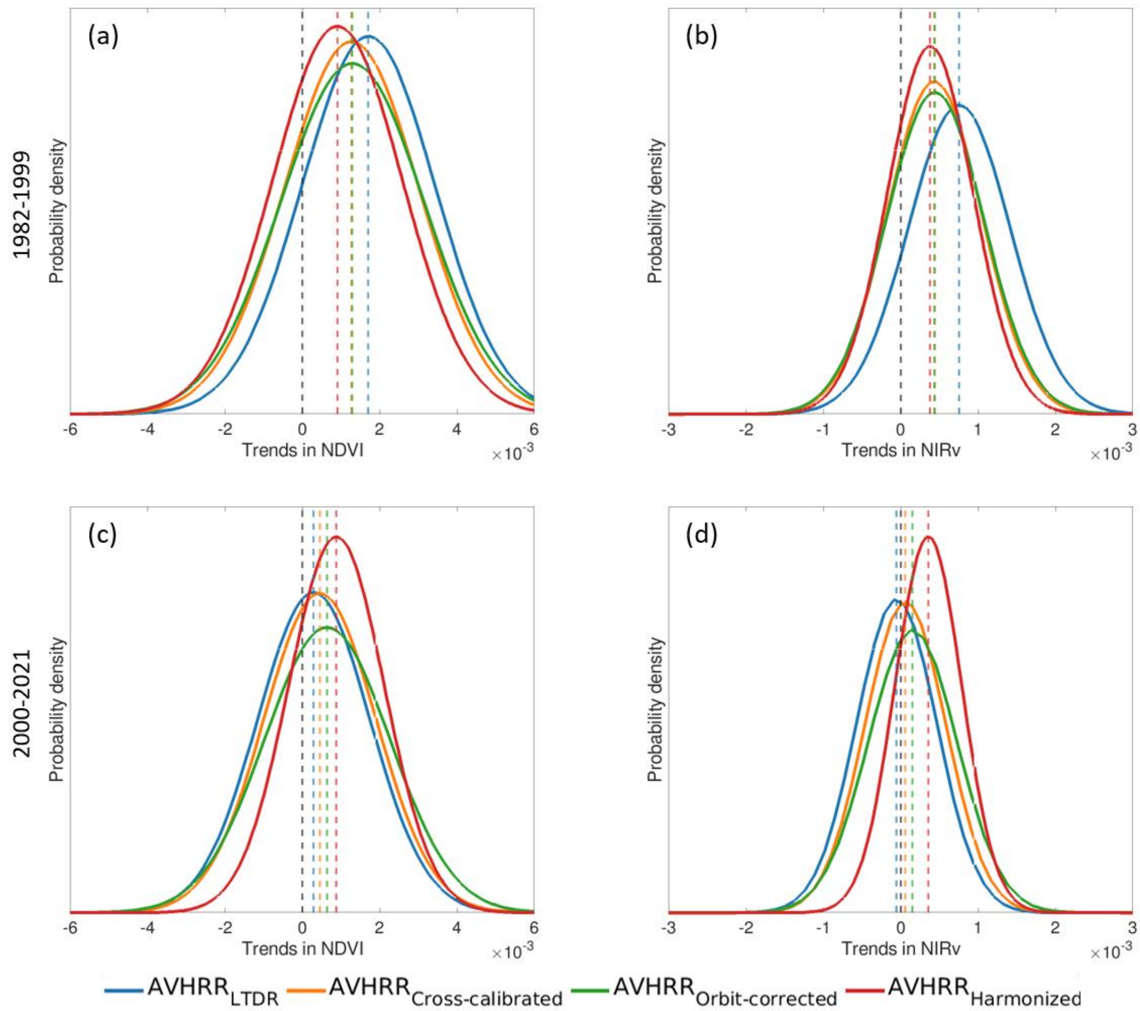

Figure A 6 Probability density function of long-term trends in different processing levels of AVHRR NDVI (a,c), and NIRv (b,d). The different colors represent original LTDR (blue), cross-calibrated (orange), orbit-corrected (green), and harmonized (red) NDVI and NIRv, respectively. The colored vertical lines indicate the averaged trends in each data.

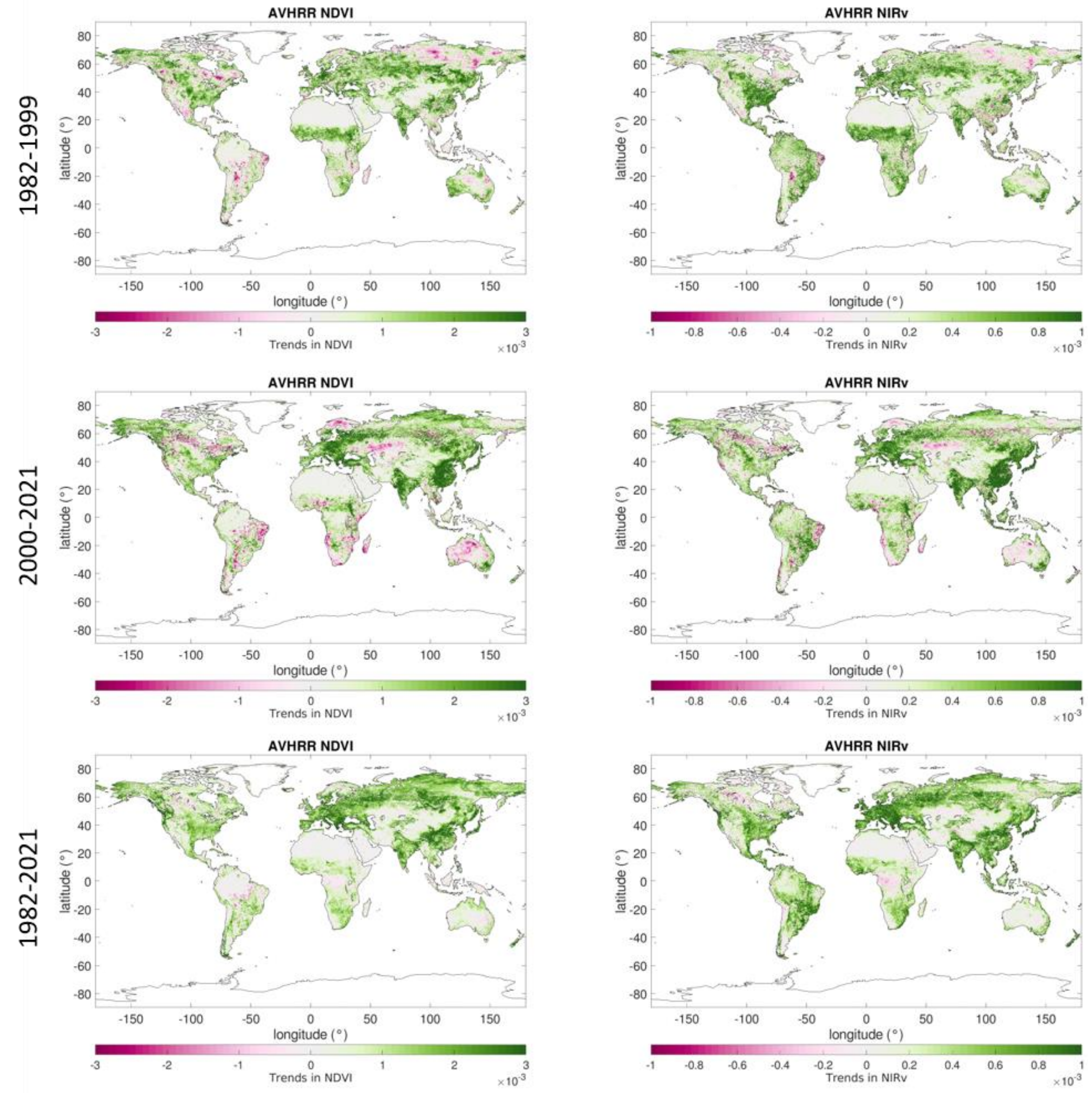

Figure A 7 Spatial patterns of trends in harmonized NDVI and NIRv. Statistically significant trends (Mann–Kendall test, p<0.1) are color-coded. Grey areas show vegetated land with statistically insignificant trends.

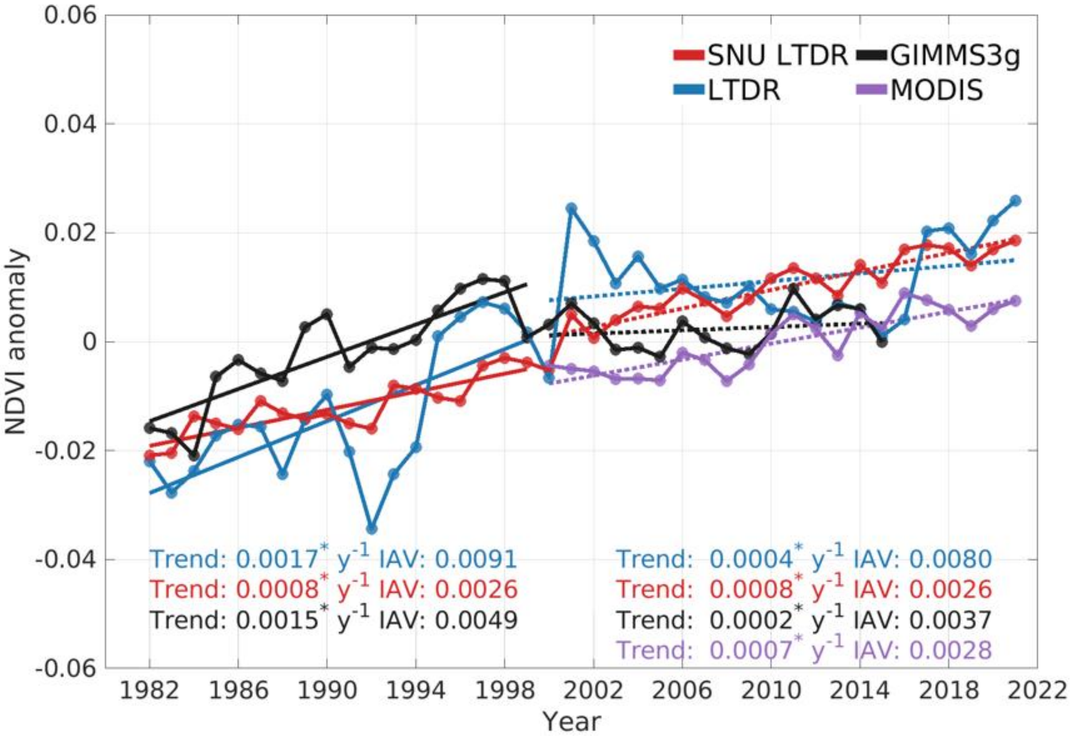

Figure A 8 Annual growing season anomaly of four NDVI datasets (AVHRR$_{LTDR}$, AVHRR$_{harmonized}$, GIMMS3g, and MODIS). Slope and interannual variability were calculated in different periods (Upper left: 1982-1999; Below right: 2000-2021; GIMMS3g: 2000-2015). The different colors represent AVHRR$_{LTDR}$ (LTDR) (blue), AVHRR$_{harmonized}$ (SNU LTDR) (orange), GIMMS3g (green), and MODIS (purple) NDVI, respectively.

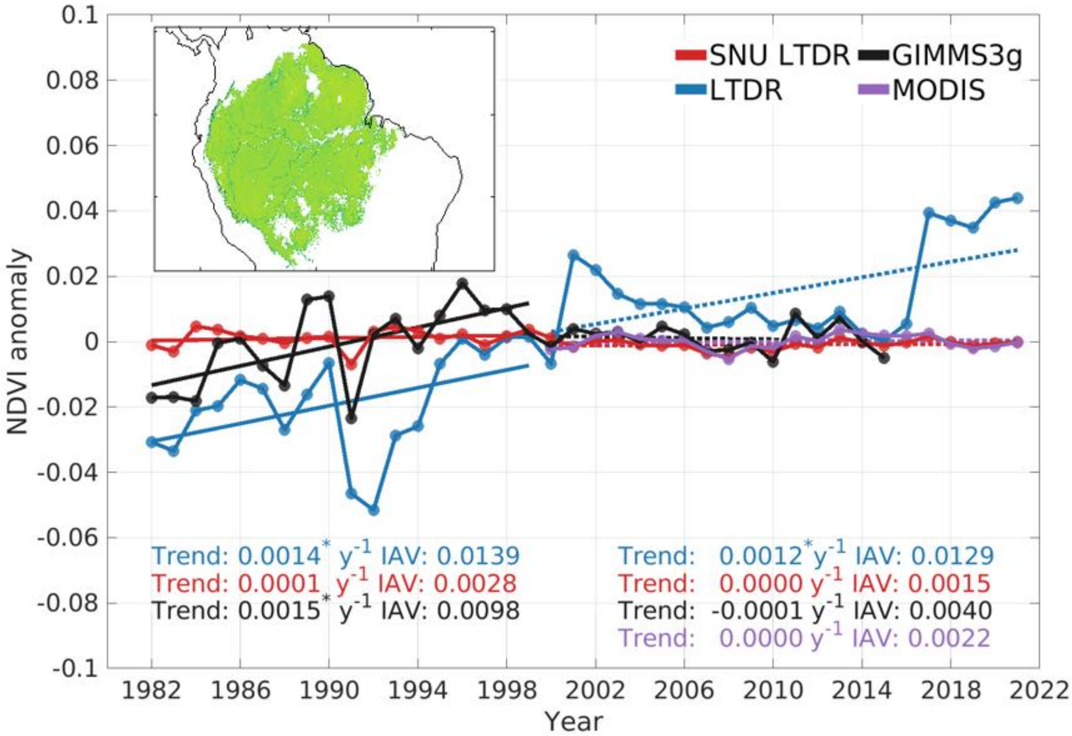

Figure A 9 Annual growing season anomaly of four NDVI datasets in Amazon evergreen broadleaf forests ($AVHRR_{LTDR}$, $AVHRR_{harmonized}$, GIMMS3g, and MODIS). Slope and interannual variability were calculated in different periods (Upper left: 1982-1999; Below right: 2000-2021; GIMMS3g: 2000-2015). The different colors represent $AVHRR_{LTDR}$ (LTDR) (blue), $AVHRR_{harmonized}$ (SNU LTDR) (orange), GIMMS3g (green), and MODIS (purple) NDVI, respectively.

6 Reference

Bacour, C., Briottet, X., Bréon, F. M., Viallefont-Robinet, F., & Bouvet, M. (2019). Revisiting Pseudo Invariant Calibration Sites (PICS) over sand deserts for vicarious calibration of optical imagers at 20 km and 100 km scales. Remote Sensing, 11(10), 1166.

Badgley, G., Field, C. B., & Berry, J. A. (2017). Canopy near-infrared reflectance and terrestrial photosynthesis. Science advances, 3(3), e1602244.

Baret, F., Hagolle, O., Geiger, B., Bicheron, P., Miras, B., Huc, M., ... & Leroy, M. (2007). LAI, fAPAR and fCover CYCLOPES global products derived from VEGETATION: Part 1: Principles of the algorithm. Remote sensing of environment, 110(3), 275-286.

Berner, L. T., Massey, R., Jantz, P., Forbes, B. C., Macias-Fauria, M., Myers-Smith, I., ... & Goetz, S. J. (2020). Summer warming explains widespread but not uniform greening in the Arctic tundra biome. Nature Communications, 11(1), 4621.

Bhatt, R., Doelling, D. R., Scarino, B. R., Gopalan, A., Haney, C. O., Minnis, P., & Bedka, K. M. (2016). A consistent AVHRR visible calibration record based on multiple methods applicable for the NOAA degrading orbits. Part I: Methodology. Journal of Atmospheric and Oceanic Technology, 33(11), 2499-2515.

Chen, C., Park, T., Wang, X., Piao, S., Xu, B., Chaturvedi, R. K., ... & Myneni, R. B. (2019). China and India lead in greening of the world through land-use management. Nature sustainability, 2(2), 122-129.

Chen, C., Park, T., Wang, X., Piao, S., Xu, B., Chaturvedi, R. K., ... & Myneni, R. B. (2019). China and India lead in greening of the world through land-use management. Nature sustainability, 2(2), 122-129.

Defourny, P., Kirches, G., Brockmann, C., Boettcher, M., Peters, M., Bontemps, S., ... & Santoro, M. (2012). Land cover CCI. Product User Guide Version, 2, 325.

Fan, X., & Liu, Y. (2016). A global study of NDVI difference among moderate-resolution satellite sensors. ISPRS Journal of Photogrammetry and Remote Sensing, 121, 177-191.

Fang, W., Huang, S., Huang, Q., Huang, G., Wang, H., Leng, G., ... & Guo, Y. (2019). Probabilistic assessment of remote sensing-based terrestrial vegetation vulnerability to drought stress of the Loess Plateau in China. Remote sensing of environment, 232, 111290.

Fensholt, R., & Proud, S. R. (2012). Evaluation of earth observation based global long term vegetation trends—Comparing GIMMS and MODIS global NDVI time series. Remote sensing of Environment, 119, 131-147.

Fensholt, R., Rasmussen, K., Nielsen, T. T., & Mbow, C. (2009). Evaluation of earth observation based long term vegetation trends—Intercomparing NDVI time series trend analysis consistency of Sahel from AVHRR GIMMS, Terra MODIS and SPOT VGT data. Remote sensing of environment, 113(9), 1886-1898.

Franch, B., Vermote, E. F., Roger, J. C., Murphy, E., Becker-Reshef, I., Justice, C., ... & Devadiga, S. (2017). A 30+ year AVHRR land surface reflectance climate data record and its application to wheat yield monitoring. Remote Sensing, 9(3), 296.

Frankenberg, C., Yin, Y., Byrne, B., He, L., & Gentine, P. (2021). Comment on "Recent global decline of CO2 fertilization effects on vegetation photosynthesis". Science, 373(6562), eabg2947.

Gao, F., Anderson, M. C., Kustas, W. P., & Wang, Y. (2012). Simple method for retrieving leaf area index from Landsat using MODIS leaf area index products as reference. Journal of Applied Remote Sensing, 6(1), 063554-063554.

Giglio, L., & Roy, D. P. (2020). On the outstanding need for a long-term, multi-decadal, validated and quality assessed record of global burned area: Caution in the use of Advanced Very High Resolution Radiometer data. Science of Remote Sensing, 2, 100007.

Giglio, L., & Roy, D. P. (2022). Assessment of satellite orbit-drift artifacts in the long-term AVHRR FireCCILT11 global burned area data set. Science of Remote Sensing, 5, 100044.

Hashimoto, H., Wang, W., Dungan, J. L., Li, S., Michaelis, A. R., Takenaka, H., ... & Nemani, R. R. (2021). New generation geostationary satellite observations support seasonality in greenness of the Amazon evergreen forests. Nature Communications, 12(1), 684.

Hersbach, H., Bell, B., Berrisford, P., Hirahara, S., Horányi, A., Muñoz-Sabater, J., ... & Thépaut, J. N. (2020). The ERA5 global reanalysis. Quarterly Journal of the Royal Meteorological Society, 146(730), 1999-2049.

Jeong, S., Ryu, Y., Dechant, B., Li, X., Kong, J., Choi, W., ... & Chun, J. (2023). Tracking diurnal to seasonal variations of gross primary productivity using a geostationary satellite, GK-2A advanced meteorological imager. Remote Sensing of Environment, 284, 113365.

Jiang, C., Ryu, Y., Fang, H., Myneni, R., Claverie, M., & Zhu, Z. (2017). Inconsistencies of interannual variability and trends in long-term satellite leaf area index products. Global Change Biology, 23(10), 4133-4146.

Julien, Y., & Sobrino, J. A. (2012). Correcting AVHRR Long Term Data Record V3 estimated LST from orbital drift effects. Remote sensing of environment, 123, 207-219.

Keenan, T. F., Prentice, I. C., Canadell, J. G., Williams, C. A., Wang, H., Raupach, M., & Collatz, G. J. (2016).

Recent pause in the growth rate of atmospheric CO2 due to enhanced terrestrial carbon uptake. Nature communications, 7(1), 13428.

Knyazikhin, Y., Martonchik, J. V., Myneni, R. B., Diner, D. J., & Running, S. W. (1998). Synergistic algorithm for estimating vegetation canopy leaf area index and fraction of absorbed photosynthetically active radiation from MODIS and MISR data. Journal of Geophysical Research: Atmospheres, 103(D24), 32257-32275.

Kolby Smith, W., Reed, S. C., Cleveland, C. C., Ballantyne, A. P., Anderegg, W. R., Wieder, W. R., ... & Running, S. W. (2016). Large divergence of satellite and Earth system model estimates of global terrestrial CO2 fertilization. Nature climate change, 6(3), 306-310.

Latifovic, R., Pouliot, D., & Dillabaugh, C. (2012). Identification and correction of systematic error in NOAA AVHRR long-term satellite data record. Remote Sensing of Environment, 127, 84-97.

Li, C., Xue, Y., Liu, Q., Guang, J., He, X., Zhang, J., ... & Liu, X. (2014). Post calibration of channels 1 and 2 of long-term AVHRR data record based on SeaWiFS data and pseudo-invariant targets. Remote sensing of environment, 150, 104-119.

Li, M., Cao, S., Zhu, Z., Wang, Z., Myneni, R. B., & Piao, S. (2023). Spatiotemporally consistent global dataset of the GIMMS Normalized Difference Vegetation Index (PKU GIMMS NDVI) from 1982 to 2022. Earth System Science Data, 15(9), 4181-4203.

Li, X., Xiao, J., Fisher, J. B., & Baldocchi, D. D. (2021). ECOSTRESS estimates gross primary production with fine spatial resolution for different times of day from the International Space Station. Remote Sensing of Environment, 258, 112360.

Liu, Y., Liu, R., & Chen, J. M. (2012). Retrospective retrieval of long-term consistent global leaf area index (1981-2011) from combined AVHRR and MODIS data. Journal of Geophysical Research: Biogeosciences, 117(G4).

Los, S. O. (1998). Estimation of the ratio of sensor degradation between NOAA AVHRR channels 1 and 2 from monthly NDVI composites. IEEE Transactions on Geoscience and Remote Sensing, 36(1), 206-213.

Mao, D., Wang, Z., Luo, L., & Ren, C. (2012). Integrating AVHRR and MODIS data to monitor NDVI changes and their relationships with climatic parameters in Northeast China. International Journal of Applied Earth Observation and Geoinformation, 18, 528-536.

Miura, T., Smith, C. Z., & Yoshioka, H. (2021). Validation and analysis of Terra and Aqua MODIS, and SNPP VIIRS vegetation indices under zero vegetation conditions: A case study using Railroad Valley Playa. Remote Sensing of Environment, 257, 112344.

Myneni, R. B., Hoffman, S., Knyazikhin, Y., Privette, J. L., Glassy, J., Tian, Y., ... & Running, S. W. (2002). Global products of vegetation leaf area and fraction absorbed PAR from year one of MODIS data. Remote sensing of environment, 83(1-2), 214-231.

Myneni, R. B., Ramakrishna, R., Nemani, R., & Running, S. W. (1997). Estimation of global leaf area index and absorbed PAR using radiative transfer models. IEEE Transactions on Geoscience and remote sensing, 35(6), 1380-1393.

Nagol, J. R., Vermote, E. F., & Prince, S. D. (2014). Quantification of impact of orbital drift on inter-annual trends in AVHRR NDVI data. Remote Sensing, 6(7), 6680-6687.

Otón, G., Lizundia-Loiola, J., Pettinari, M. L., & Chuvieco, E. (2021). Development of a consistent global long-term burned area product (1982–2018) based on AVHRR-LTDR data. International Journal of Applied Earth Observation and Geoinformation, 103, 102473.

Pedelty, J., Devadiga, S., Masuoka, E., Brown, M., Pinzon, J., Tucker, C., ... & Pinheiro, A. (2007, July). Generating a long-term land data record from the AVHRR and MODIS instruments. In 2007 IEEE international Geoscience and remote sensing Symposium (pp. 1021-1025). IEEE.

Piao, S., Wang, X., Park, T., Chen, C., Lian, X. U., He, Y., ... & Myneni, R. B. (2020). Characteristics, drivers and feedbacks of global greening. Nature Reviews Earth & Environment, 1(1), 14-27.

Pinzon, J. E., & Tucker, C. J. (2014). A non-stationary 1981–2012 AVHRR NDVI3g time series. Remote sensing, 6(8), 6929-6960.

Privette, J. L., Fowler, C., Wick, G. A., Baldwin, D., & Emery, W. J. (1995). Effects of orbital drift on advanced very high resolution radiometer products: Normalized difference vegetation index and sea surface temperature. Remote Sensing of Environment, 53(3), 164-171.

Quinlan, J. R. (1992, November). Learning with continuous classes. In 5th Australian joint conference on artificial intelligence (Vol. 92, pp. 343-348).

Randles, C. A., Da Silva, A. M., Buchard, V., Colarco, P. R., Darmenov, A., Govindaraju, R., ... & Flynn, C. J. (2017). The MERRA-2 aerosol reanalysis, 1980 onward. Part I: System description and data assimilation evaluation. Journal of climate, 30(17), 6823-6850.

Roerink, G. J., Menenti, M., & Verhoef, W. (2000). Reconstructing cloudfree NDVI composites using Fourier analysis of time series. International Journal of Remote Sensing, 21(9), 1911-1917.

Roujean, J. L., Leroy, M., & Deschamps, P. Y. (1992). A bidirectional reflectance model of the Earth's surface for the correction of remote sensing data. Journal of Geophysical Research: Atmospheres, 97(D18), 20455-20468.

Ryu, Y., Berry, J. A., & Baldocchi, D. D. (2019). What is global photosynthesis? History, uncertainties and opportunities. Remote sensing of environment, 223, 95-114.

Santamaria-Artigas, A., Vermote, E. F., Franch, B., Roger, J. C., & Skakun, S. (2021). Evaluation of the AVHRR surface reflectance long term data record between 1984 and 2011. International Journal of Applied Earth Observation and Geoinformation, 98, 102317.

Schaaf, C. B., Gao, F., Strahler, A. H., Lucht, W., Li, X., Tsang, T., ... & Roy, D. (2002). First operational BRDF, albedo nadir reflectance products from MODIS. Remote sensing of Environment, 83(1-2), 135-148.

Tian, F., Fensholt, R., Verbesselt, J., Grogan, K., Horion, S., & Wang, Y. (2015). Evaluating temporal consistency of long-term global NDVI datasets for trend analysis. Remote Sensing of Environment, 163, 326-340.

Tucker, C. J. (1979). Red and photographic infrared linear combinations for monitoring vegetation. Remote sensing of Environment, 8(2), 127-150.

Tucker, C. J., Pinzon, J. E., Brown, M. E., Slayback, D. A., Pak, E. W., Mahoney, R., ... & El Saleous, N. (2005). An extended AVHRR 8-km NDVI dataset compatible with MODIS and SPOT vegetation NDVI data. International journal of remote sensing, 26(20), 4485-4498.

Verhoef, W. (1996). Application of harmonic analysis of NDVI time series (HANTS). Fourier analysis of temporal NDVI in the Southern African and American continents, 108, 19-24.

Vermote, E. (2021). LTDR AVHRR Products (Version 5) User's Guide

Vermote, E. F., & Kotchenova, S. (2008). Atmospheric correction for the monitoring of land surfaces. Journal of Geophysical Research: Atmospheres, 113(D23).

Vermote, E. F., & Saleous, N. Z. (2006). Calibration of NOAA16 AVHRR over a desert site using MODIS data. Remote sensing of Environment, 105(3), 214-220.

Vermote, E. F., El Saleous, N., Justice, C. O., Kaufman, Y. J., Privette, J. L., Remer, L., ... & Tanre, D. (1997). Atmospheric correction of visible to middle-infrared EOS-MODIS data over land surfaces: Background, operational algorithm and validation. Journal of Geophysical Research: Atmospheres, 102(D14), 17131-17141.

Vermote, E., & Kaufman, Y. J. (1995). Absolute calibration of AVHRR visible and near-infrared channels using ocean and cloud views. International Journal of Remote Sensing, 16(13), 2317-2340.

Vermote, E., Justice, C. O., & Bréon, F. M. (2008). Towards a generalized approach for correction of the BRDF effect in MODIS directional reflectances. IEEE Transactions on Geoscience and Remote Sensing, 47(3), 898-908.

Villaescusa-Nadal, J. L., Franch, B., Roger, J. C., Vermote, E. F., Skakun, S., & Justice, C. (2019). Spectral adjustment model's analysis and application to remote sensing data. IEEE Journal of Selected Topics in Applied Earth Observations and Remote Sensing, 12(3), 961-972.

Wang, X., Xiao, J., Li, X., Cheng, G., Ma, M., Zhu, G., ... & Jassal, R. S. (2019). No trends in spring and autumn phenology during the global warming hiatus. Nature Communications, 10(1), 2389.

Wang, Z., Schaaf, C. B., Sun, Q., Shuai, Y., & Román, M. O. (2018). Capturing rapid land surface dynamics with Collection V006 MODIS BRDF/NBAR/Albedo (MCD43) products. Remote sensing of environment, 207, 50-64.

Wanner, W., Li, X., & Strahler, A. H. (1995). On the derivation of kernels for kernel-driven models of bidirectional reflectance. Journal of Geophysical Research: Atmospheres, 100(D10), 21077-21089.

Xiao, J., Zhuang, Q., Baldocchi, D. D., Law, B. E., Richardson, A. D., Chen, J., ... & Torn, M. S. (2008). Estimation of net ecosystem carbon exchange for the conterminous United States by combining MODIS and AmeriFlux data. Agricultural and Forest Meteorology, 148(11), 1827-1847.

Xiao, Z., Liang, S., Wang, J., Xiang, Y., Zhao, X., & Song, J. (2016). Long-time-series global land surface satellite leaf area index product derived from MODIS and AVHRR surface reflectance. IEEE Transactions on Geoscience and Remote Sensing, 54(9), 5301-5318.

Zeng, Y., Hao, D., Huete, A., Dechant, B., Berry, J., Chen, J. M., ... & Chen, M. (2022). Optical vegetation indices for monitoring terrestrial ecosystems globally. Nature Reviews Earth & Environment, 3(7), 477-493.

Zhang, Y., Song, C., Band, L. E., Sun, G., & Li, J. (2017). Reanalysis of global terrestrial vegetation trends from MODIS products: Browning or greening?. Remote Sensing of Environment, 191, 145-155.

Zhou, J., Jia, L., & Menenti, M. (2015). Reconstruction of global MODIS NDVI time series: Performance of Harmonic ANalysis of Time Series (HANTS). Remote Sensing of Environment, 163, 217-228.

Zhu, Z., Bi, J., Pan, Y., Ganguly, S., Anav, A., Xu, L., ... & Myneni, R. B. (2013). Global data sets of vegetation leaf area index (LAI) 3g and fraction of photosynthetically active radiation (FPAR) 3g derived from global inventory modeling and mapping studies (GIMMS) normalized difference vegetation index (NDVI3g) for the period 1981 to 2011. Remote sensing, 5(2), 927-948.

Zhu, Z., Piao, S., Myneni, R. B., Huang, M., Zeng, Z., Canadell, J. G., ... & Zeng, N. (2016). Greening of the Earth and its drivers. Nature climate change, 6(8), 791-795.

Zhu, Z., Zeng, H., Myneni, R. B., Chen, C., Zhao, Q., Zha, J., ... & MacLachlan, I. (2021). Comment on “Recent global decline of CO2 fertilization effects on vegetation photosynthesis”. Science, 373(6562), eabg5673.